



Hochschule
Bonn-Rhein-Sieg
University of Applied Sciences

b-it
Bonn-Aachen
International Center for
Information Technology



Master's Thesis

“On the Explainability of Neural Network Models to Classify Rare Genetic Syndromes from Frontal Facial Images”

Aswinkumar Vijayananth

Submitted to Hochschule Bonn-Rhein-Sieg,
Department of Computer Science
in partial fulfilment of the requirements for the degree
of Master of Science in Autonomous Systems

Supervised by

Prof. Dr Paul G. Plöger
Prof. Dr Ralf Thiele
Prof. Dr. med. Dipl. Phys. Peter Krawitz

November 2022

I, the undersigned below, declare that this work has not previously been submitted to this or any other university and that it is, unless otherwise stated, entirely my own work.

Date

Aswinkumar Vijayananth

Abstract

Your abstract

Acknowledgements

Thanks to

Contents

List of Figures	xiii
List of Tables	xv
1 Introduction	1
1.1 Motivation	2
1.2 Importance	2
1.3 Challenges and Difficulties	3
1.4 Problem Statement	4
1.5 Structure	5
2 Background	7
2.1 Rare Genetic Syndromes	8
2.2 Phenotypes	8
2.3 Human Phenotype Ontology	8
3 State of the Art	9
3.1 Explainability Methods for Neural Networks	9
3.2 Input Attribution Methods	9
3.2.1 Occlusion Sensitivity Maps	9
3.2.2 Deconvolution	10
3.2.3 Saliency Maps	11
3.2.4 Guided Backpropagation	12
3.2.5 Deep LIFT	13
3.3 Layer-wise Relevance Propagation	14
3.4 Layer Attribution Methods	14
3.4.1 GradCAM	14
3.4.2 HiResolution Class Activation Mapping (HiResCAM)	15
3.4.3 Full-Grad	16
4 Methodology	19
4.1 Datasets	19
4.2 Selection of Methods	19
4.2.1 More Reasons to Consider Layer Attribution Methods	20
4.3 Design of Experiments	21
4.4 Evaluation	23

4.4.1	Objective Measures	23
4.4.2	Rationale to Adopt Subjective Evaluation	24
4.4.3	Proposed Evaluation Procedure	24
5	Implementation	29
5.1	GestaltMatcher Architecture	29
5.2	Explanation Methods - GestaltMatcher Integration	30
5.2.1	Visualization Details	33
5.3	Experiments	33
5.3.1	Patient-wise Attribution Map Generation	34
5.3.2	Composite Face Generation	34
5.3.3	Syndrome-wise Attribution Map Generation	35
5.3.4	Dataset Imbalance - Explanation Quality Analysis	37
5.4	Evaluation Questionnaire	37
6	Evaluation and Results	39
6.1	Metrics	39
6.2	Qualitative Analysis	39
6.2.1	Patient-wise Maps	39
6.2.2	Syndrome-wise Maps	39
6.2.3	Composite Faces	39
6.3	Effect of Class Imbalance on the Explainability of Models	39
6.4	Quantitative Analysis	39
6.4.1	Use of Occlusion Sensitivity Maps	39
6.4.2	Eye-tracking based Evaluation	39
6.4.3	Similarity Mapping	39
6.5	Evaluation Summary	39
7	Conclusions	41
7.1	Contributions	41
7.2	Lessons learned	41
7.3	Future work	41
Appendix A	Design Details	43
Appendix B	Parameters	45
References		47

List of Figures

3.1 An illustration of occlusion sensitivity mapping	11
4.1 An example showing input attribution maps of discussed methods, generated for a patient image	21
4.2 An example for layer attribution maps of discussed methods, generated for a patient image	21
4.3 Design of experiments	22
4.4 Proposed procedure to evaluate patient-wise attribution maps	25
4.5 Proposed procedure to evaluate composite faces	26
4.6 Proposed procedure to evaluate composite faces	27
5.1 Illustration of the pipeline to process a patient photo using GestaltMatcher	29
5.3 An illustration of attribution map computation from the GestaltMatcher model	30
5.2 Architecture of the CNN in GestaltMatcher. The convolution layer 14 used to generate attribution maps using GradCAM and HiResCAM methods is highlighted using a blue box. Layers (10.a, 11.a and 14) that are used by the CustomGradCAM method are highlighted using cyan boxes.	31
5.4 Layer-wise visualization of attribution maps generated by GradCAM and HiResCAM methods.	32
5.5 An example for patient-wise attribution maps	34
5.6 Block diagram representing composite face generation process	34
5.7 An example for syndrome-wise attribution maps	37

List of Tables

1

Introduction

“Artificial Neural Networks (ANNs) are increasingly applied for medical image diagnostics” [1]. Medical image data such as scans produced from imaging devices like x-rays [2], Magnetic Resonance Imaging (MRI) [3], Computed Tomography (CT) [4], and ultra sound [5], waveforms produced from procedures like ElectroCardioGraphy (ECG) [6] and ElectroEncephaloGraphy (EEG), histological images [7], images of body parts, and admission notes [8] are fed into ANNs to perform tasks such as segmentation [9], classification [10] and abnormality detection [7].

Predictions made by neural network models are typically intended to be used in a clinical setting, to aid medical practitioners in diagnosing their patients. As a result, it can help in an overall reduction of “misdiagnosis”, which is one of the most severe problems in health care [8]. Besides, the adoption of ANN based Artificial Intelligence (AI) systems facilitates early screening and identification of life-threatening conditions such as cancer in population with limited or no access to sub-specialty trained clinicians.

ANN models such as the ones used in AI systems for intracranial haemorrhage classification [4] and breast cancer prediction [11] are claimed to outperform clinicians in their respective tasks. In spite of their success in terms of predictive performance, the black box nature of ANNs restrains them from getting deployed in a clinical setting. Inherently, ANNs lack transparency and therefore are considered to be less dependable for high stake applications like medical diagnosis and autonomous driving. Besides, regulatory bodies such as “US FDA (United States Food and Drug Administration) require any clinical decision support software to explain the rationale or support for its decisions to enable the users to independently review the basis of their recommendations” [4]. Such contradictions further restrict the deployment of ANN based AI systems for performing medical diagnoses in a clinical setting.

“Explainable Artificial Intelligence (XAI) is a set of processes and methods that allows human users to comprehend and trust the results and output created by machine learning algorithms” [12]. Application of XAI techniques to Machine Learning (ML) models enables its human users to better understand their behavior and rationale behind their predictions. As a result, they improve transparency of models like ANNs, in turn making them more trustworthy for applications like medical diagnosis.

In the recent times, there has been a steep rise in the adoption of XAI methods to explain ANN models for medical diagnoses. A considerable number existing works focus on explaining neural network models that use radiological image data to perform tasks such as COVID classification [13], breast cancer risk assessment [5] and haemorrhage detection [4] respectively. A few other leverage XAI techniques to explain

neural network models used for detecting cancer from histopathological [7] and skin images [14].

The objective of this thesis is to use XAI to explain one such neural network model called GestaltMatcher [15], which surpasses the performance of clinical practitioners in the identification of certain rare genetic syndromes, from frontal facial images of patients. The findings of this work shall make the GestaltMatcher model more transparent and dependable, thereby taking it a step closer to be deployed in a clinical setting.

1.1 Motivation

“Rare genetic disorders affect more than 6.2% of global population” [15]. A significant fraction of the population with certain such disorders are characterized by facial abnormalities, which make up their respective facial phenotypes. The facial phenotypic information is used by clinical geneticists along with results from other laboratory tests such as molecular, to reach a diagnosis. However, the rarity in occurrence of such disorders combined with the lack of distinctive traits for a subset of them, makes their diagnosis a challenging task even for experienced medical practitioners.

ANN models such as the ones presented in DeepGestalt [10] and GestaltMatcher [15] comprise a promising step forward in using AI for the task of recognizing rare genetic disorders from facial phenotypes. Such works rely on databases like Face2Gene [16] and GestaltMatcher database (GMDB) [17] which offer a valuable collection of frontal facial images and other medical data of the patients with such rare disorders. The GestaltMatcher [15] model surpasses human expert’s performance in the task of recognizing certain syndromes and their sub types. Therefore, deployment of such models in a clinical setting has the potential to significantly improve the speed and accuracy of diagnoses.

The constraints on deploying ANN models for medical diagnoses in a clinical setting, as discussed in the previous section, apply to the genetic disorder classifiers as well. Therefore, there is an obligation for such models to provide bases for their predictions in order to make them dependable. However, none of the existing works on genetic disorder classification from frontal facial images focus on the explainability of their models.

In general, ANN models are capable of learning novel discriminative features or regions from the training data, that are relevant to the task at hand. Associating such learned features or regions with the real world knowledge (with respect to the dataset) can provide new insights about the data and task at hand. In the case of genetic disorder classification, associating attention regions of SOTA models like DeepGestalt [10] and GestaltMatcher [15] in their frontal facial input images can enhance human kind’s understanding about facial phenotypes of genetic disorders. Such a study to associate the attention regions of genetic disorder classifiers with the facial phenotypic information known to the medical community, is yet to be conducted.

1.2 Importance

Making a genetic disorder classifier explainable by determining its attention regions, offers a means for its users to check whether the model focuses on features relevant to a given disorder, or something irrelevant like background, for example. In the former case, a clinician could use the model’s prediction to reinforce their diagnoses. In the latter, they could simply ignore its decisions. Thus an explainable genetic disorder classifier provides a verifiable second opinion to a clinical geneticist.

The knowledge about facial phenotypes of rare genetic disorders are contained in resources like Human Phenotype Ontology (HPO) [18] and relevant medical literature. However, due to rare occurrences of such disorders, not all variations in their phenotypes are known to the medical community. Analyzing the attention regions of genetic disorder classifier models offers a way to discover facial regions that contain novel phenotypic traits, thereby enhancing human kind's understanding of such rare medical conditions.

Datasets like GMDB [17] only contain a fractional number of instances per class, when compared with sizes of general purpose image classification datasets like ImageNet [19]. Most of the disorder classes contains samples in the order of tens and a few in the order of hundreds. This in turn demands use of highly effective data pre-processing and model training techniques to learn the most from a dataset. Analyzing attention regions of a classifier model trained on such datasets, enables an ML practitioner to identify any possible biases that the model could have learned, and consecutively enables him to adopt suitable techniques to remove them. This eventually makes the model more generalized and possibly increases its predictive performance.

1.3 Challenges and Difficulties

This section lists and discusses some of the key challenges associated with this research work.

- **Dataset size and imbalance:** As briefly mentioned in the previous section, datasets like GMDB [15] are small-sized, and also are characterized by problems such as dataset imbalance and low image resolution. Figure ?? depicts the class-wise distribution of samples in GMDB. Such problems are caused by various factors like inherent rarity in occurrence of genetic syndromes, data-privacy constraints and lack of openly available datasets. The above listed issues of genetic syndrome datasets often have consequential effects on the performance and explainability of machine learning models they are trained with.
- **Low predictive performance of the classifier:** Although, SOTA genetic syndrome classifier models such as DeepGestalt [10] and GestaltMatcher [15] surpass human-level performance in diagnosing rare genetic disorders, their predictive performances are exceptionally low when compared with that of top classification models trained on large general purpose datasets. Besides, over-fitting is a common problem experienced by these models. In most of the existing works on XAI methods for neural networks, the research community has benchmarked them on high performance models. This raises doubts about the quality of explanations generated by XAI methods, when applied to low performance models.
- **Lack of ground truth explanations:** Evaluating the performance and effectiveness of XAI methods remains a challenge till date. In most of the cases, this is due to the lack of any ground truth and/or metrics to evaluate their explanations. Besides, the working principle of every XAI method is different, with each focusing on explaining a particular aspect of model and its predictions. Due to this reason, often XAI methods are evaluated by subjecting their corresponding artifacts to be assessed by humans. In the case of this work, such an evaluation needs to be performed by clinicians and dysmorphologists who specialize in the diagnosis of rare genetic syndromes. Certain

practical difficulties in conducting such an evaluation like the willingness of clinicians to participate in the process pose a challenge. In addition, new findings and discoveries about phenotypic features and new variants of genetic syndromes change the medical community's understanding of them time to time, questioning the correctness of clinical evaluation conducted at a given point in time.

1.4 Problem Statement

This research work systematically approaches the problem in hand. Firstly, a literature review is conducted to identify SOTA XAI methods, which when applied to the GestaltMatcher model explains the rationale behind its predictions, in the form of post-hoc attention maps. In a classification setup, post-hoc attention heat maps such as the ones in Figure ??, signal regions in the input image that were relevant for a classifier model to produce a certain class label. A handful of XAI methods are shortlisted based on their advantages and drawbacks, recommendations from the research community, and their suitability to the task at hand.

The selected set of techniques are applied to GestaltMatcher [15], in order to generate explanations associated with the model's predictions for every patient image in the GMDB [15] dataset. The generated explanations are then analyzed with intents to understand the behaviours of both the model and the chosen set of XAI techniques with different input categories. Besides analyzing the model's regions of interest in individual patient images, this work also studies its characteristic attention regions on a class level for specific syndromes. Such characteristic representations are produced by combining patient-wise attention maps of individual classes.

As mentioned in 1.3, dataset imbalance is one of the key challenges in the application of machine learning techniques to medical data. This can have consequences on the quality of attention maps generated for classes of different sizes. This work conducts experiments to analyze the effects of class imbalance on the quality of explanation artifacts. This is achieved by comparing attention maps, produced from classifier models that are trained with different numbers and choices for the syndrome classes.

Inorder to know the association between GestaltMatcher's attention regions and the medical community's knowledge on facial phenotypic features of genetic syndromes, the model's attention maps need to be evaluated by clinicians. It is a time-consuming process which involves the participation of atleast a few dysmorphologists and sub-specialty trained clinicians. Such an evaluation is not included in this work, due to the time constraints, however, a questionnaire to facilitate the process in future is formulated and presented. Besides, this thesis also suggests and proposes ways to quantitatively evaluate the attention maps.

Finally, a use case scenario is presented, depicting the application of techniques presented in this work to a real-world genetic syndrome diagnosis situation.

Research Questions

Concisely put, this thesis intends to address the following research questions:

RQ1. What are the XAI methods to determine important regions in an input image for a CNN based classifier model to make its predictions?

RQ2. What are the key regions in frontal facial images fed to CNN models trained for the task of classifying rare genetic disorders?

RQ3. How do the regions obtained from findings for RQ2 compare with the knowledge known to the medical community on facial phenotypes of the corresponding rare genetic disorders?

1.5 Structure

This report consists of seven chapters (including this chapter) with each discussing different aspects of the conducted research work. The first chapter introduced the reader to the research topic, and discusses the scope and significance of this work. Chapter 2 gives the necessary background knowledge of rare genetic syndromes and their diagnoses using GestaltMatcher [15], which is necessary to appreciate this work. The chapter also briefly introduces the reader to the field of XAI and discusses the taxonomy of explanation methods. In Chapter 3, a literature review of SOTA explanation methods considered for this research work is provided. Chapter 4 describes the systematic approach taken to address the problem at hand. The chapter gives the rationale behind the design of experiments and other choices made. The fifth chapter discusses implementation details and provides specifications of datasets and models used for experimentation. The results obtained from the conducted experiments are listed and analyzed in Chapter 6. Besides, it also presents and describes the formulated evaluation questionnaire. Finally, Chapter 7 concludes the report by summarizing the contributions of this project, and also discusses the possible future research directions.

2

Background

 Lorem ipsum dolor sit amet, consectetur adipiscing elit. Ut purus elit, vestibulum ut, placerat ac, adipiscing vitae, felis. Curabitur dictum gravida mauris. Nam arcu libero, nonummy eget, consectetur id, vulputate a, magna. Donec vehicula augue eu neque. Pellentesque habitant morbi tristique senectus et netus et malesuada fames ac turpis egestas. Mauris ut leo. Cras viverra metus rhoncus sem. Nulla et lectus vestibulum urna fringilla ultrices. Phasellus eu tellus sit amet tortor gravida placerat. Integer sapien est, iaculis in, pretium quis, viverra ac, nunc. Praesent eget sem vel leo ultrices bibendum. Aenean faucibus. Morbi dolor nulla, malesuada eu, pulvinar at, mollis ac, nulla. Curabitur auctor semper nulla. Donec varius orci eget risus. Duis nibh mi, congue eu, accumsan eleifend, sagittis quis, diam. Duis eget orci sit amet orci dignissim rutrum.

 Nam dui ligula, fringilla a, euismod sodales, sollicitudin vel, wisi. Morbi auctor lorem non justo. Nam lacus libero, pretium at, lobortis vitae, ultricies et, tellus. Donec aliquet, tortor sed accumsan bibendum, erat ligula aliquet magna, vitae ornare odio metus a mi. Morbi ac orci et nisl hendrerit mollis. Suspendisse ut massa. Cras nec ante. Pellentesque a nulla. Cum sociis natoque penatibus et magnis dis parturient montes, nascetur ridiculus mus. Aliquam tincidunt urna. Nulla ullamcorper vestibulum turpis. Pellentesque cursus luctus mauris.

 Nulla malesuada porttitor diam. Donec felis erat, congue non, volutpat at, tincidunt tristique, libero. Vivamus viverra fermentum felis. Donec nonummy pellentesque ante. Phasellus adipiscing semper elit. Proin fermentum massa ac quam. Sed diam turpis, molestie vitae, placerat a, molestie nec, leo. Maecenas lacinia. Nam ipsum ligula, eleifend at, accumsan nec, suscipit a, ipsum. Morbi blandit ligula feugiat magna. Nunc eleifend consequat lorem. Sed lacinia nulla vitae enim. Pellentesque tincidunt purus vel magna. Integer non enim. Praesent euismod nunc eu purus. Donec bibendum quam in tellus. Nullam cursus pulvinar lectus. Donec et mi. Nam vulputate metus eu enim. Vestibulum pellentesque felis eu massa.

 Quisque ullamcorper placerat ipsum. Cras nibh. Morbi vel justo vitae lacus tincidunt ultrices. Lorem ipsum dolor sit amet, consectetur adipiscing elit. In hac habitasse platea dictumst. Integer tempus convallis augue. Etiam facilisis. Nunc elementum fermentum wisi. Aenean placerat. Ut imperdiet, enim sed gravida sollicitudin, felis odio placerat quam, ac pulvinar elit purus eget enim. Nunc vitae tortor. Proin tempus nibh sit amet nisl. Vivamus quis tortor vitae risus porta vehicula.

 Fusce mauris. Vestibulum luctus nibh at lectus. Sed bibendum, nulla a faucibus semper, leo velit

ultricies tellus, ac venenatis arcu wisi vel nisl. Vestibulum diam. Aliquam pellentesque, augue quis sagittis posuere, turpis lacus congue quam, in hendrerit risus eros eget felis. Maecenas eget erat in sapien mattis porttitor. Vestibulum porttitor. Nulla facilisi. Sed a turpis eu lacus commodo facilisis. Morbi fringilla, wisi in dignissim interdum, justo lectus sagittis dui, et vehicula libero dui cursus dui. Mauris tempor ligula sed lacus. Duis cursus enim ut augue. Cras ac magna. Cras nulla. Nulla egestas. Curabitur a leo. Quisque egestas wisi eget nunc. Nam feugiat lacus vel est. Curabitur consectetur.

2.1 Rare Genetic Syndromes

2.2 Phenotypes

2.3 Human Phenotype Ontology

3

State of the Art

<What did the previous chapter explain?>. This chapter emphasizes on Explainable Artificial Intelligence (XAI) methods developed for convolutional neural network (CNN) models such as GestaltMatcher. The set of methods considered for this research work are categorized and explained in a concise manner.

3.1 Explainability Methods for Neural Networks

XAI methods for neural networks visualize concepts and features learned by a model, with an intent to explain its individual predictions. The knowledge contained in a CNN model and its predictions can be represented and explained, respectively, in different ways. The abstract features and concepts learned by it can be visualized using methods such as network dissection [20]. Techniques such as Testing with Concept Activation Vectors (TCAV) [21] explain a model based on user-defined concepts like a color or an object. Attribution methods provide the rationale behind a CNN model’s output by producing an attribution map, a representation in which every pixel or feature of the input image is assigned a score, based on how much it impacts the prediction.

This work uses attribution methods to understand GestaltMatcher’s regions of attention in syndromic faces, and to explain its predictions. Most of the attribution methods make use of gradient information obtained by computing the first derivative of output score with respect to value of a feature. Kokhlikyan *et al.* [22] categorize attribution methods into three groups, based on the entity to which a model’s predictions are attributed to: input/primary, layer attribution and neuron attribution. The same dimension is used to group the methods considered for this work.

3.2 Input Attribution Methods

Input or primary attribution methods evaluate contribution of each input pixel to the output of a neural network model. This section discusses six input attribution methods considered for this research work.

3.2.1 Occlusion Sensitivity Maps

Occlusion sensitivity mapping [23] is a model-agnostic perturbation based method, which generates explanations by manipulating parts of the input image. The approach is computationally expensive,

$O(\# \text{simultaneous occlusions} * \# \text{features} * \# \text{ablations_per_eval} * 1/\#\text{strides})$, and is included in this work to verify if Gestalt Matcher model is focusing on key facial features, or simply using the surrounding context to produce predictions. This is achieved by systematically occluding different portions of the input image with a black square or rectangular mask, and computing the difference in outputs (logit scores of the target class). In this work, we use a black square mask of dimensions 10x10. Important portions of the input when occluded, result in relatively larger logit score differences, than the trivial ones. The differences are plotted on the image, yielding the occlusion sensitivity maps.

3.2.2 Deconvolution

Zeiler and Fergus proposed the “Deconvolution” [23] approach to visualize and provide insights into the functions learned by intermediate layers of a CNN. It is one of the earliest attribution techniques, which produces visualizations based on computing gradient of loss function with respect to a given input. The work acts a baseline till date for development and evaluation of new pixel attribution techniques. The method uses a deconvolution counterpart for every building block of a CNN, to obtain reverse mapping from features to input pixels. The idea of deconvolution was first introduced by Zeiler et al. [24], as a way to perform unsupervised learning. In order to obtain attribution maps using the Deconvolution approach, the first step is to attach each block of convnet with its deconvolution counterpart as shown in the figure 1. Every activation except the ones belonging to the class of interest is set to zero. The activation value is then backpropagated through the deconvolution blocks such as unpooling, rectification and transposed convolution, all the way to the input layer. Deconvolution blocks act according to a pre-defined set of rules. The transposed convolution block performs the inverse of convolution operation by using transposed versions of the same filters. This is equivalent to flipping a given filter both in vertical and horizontal directions. In order to backtrack activations through max-pooling layer (.i.e. using the unpooling layer), indices corresponding to maximum activations in every layer, are first stored during the forward pass and later retrieved during the back propagation phase. However, the use of indices or switches from the forward pass, constrains the visualization on the input image [25].

Authors test their method on an AlexNet [26] trained on the ImageNet [26], Caltech-101 [27] and Caltech-256 [28] and PASCAL2012 [29] datasets. As a first step, they visualize the top 9 feature maps of the each of the first five layers, to show the proportional increase of complexity in features with respect to their receptive fields. The visualizations are obtained by backtracking the strongest activation of a feature map for most of the data samples, all the way until a given input, using the deconvolution rules. The paper also discusses about the proportionality between the time taken for a given layer to learn features and its corresponding depth. Further, it shows that features learned by top layers are more invariant to transformations like translations, rotations and scale changes.

The work evaluates itself by qualitatively comparing its resulting attribution maps with occlusion sensitivity maps. Occlusion sensitivity maps are obtained by systematically occluding portion of an image and analyzing the given classifier’s output, to determine the most discriminative regions as shown in the first image of Figure 3.1.

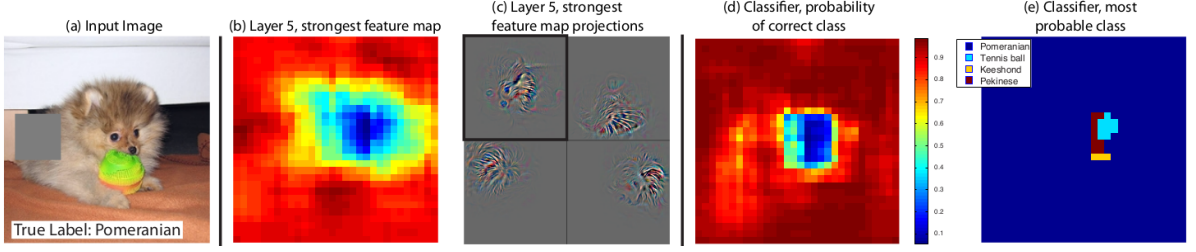


Figure 3.1: An illustration of occlusion sensitivity mapping

3.2.3 Saliency Maps

Simonyan et al. [30] propose two visualization techniques with intents to generate an image which maximizes the class score, and to compute a class-specific saliency map for a given input. The first technique numerically optimizes the input image while the other computes the spatial support of a given class in an input. This work is one of the earliest to leverage saliency maps for the task of weakly-supervised object segmentation. Authors demonstrate the proposed techniques by applying to a deep convnet trained on the ILSVRC-2013 dataset [31].

Class Model Visualization

The intention of this technique is to numerically generate an image which is representative of the target category with respect to the convolutional net’s class scoring model. This is achieved by finding a L2-regularised image such that the logit S_c of a given class c is maximized:

where λ refers to the regularization parameter and I is a local optimum, which can be found with help of back propagation. The optimization process uses the mean image of the data set as the initial value. The work also mentions about the prominence of visualizations produced by using logit scores over soft-max/unnormalized class scores.

Image-Specific Class Saliency

The objective of this technique is to rank pixels of an input image, based on their impact on class scores (S_c). Authors provide a couple of interpretations for the class score values/ logits with respect to which saliency maps are created:

1. A linear approximation of the function learned by neural network in a local neighbourhood of the input image.
2. Higher the saliency associated with a pixel, lesser it needs to be altered in order to increase its respective class’s score.

The derivative of class score with respect to input image is found using back propagation as described by the equation below:

In order to obtain the saliency map for a multi-channel image, the maximum magnitude of gradient for a given position across channels is used. Class saliency maps thus produced are used as initial points to compute object segmentation mask using the GraphCut algorithm [32]. Foreground and background portions are considered as Gaussian Mixture Models and the former is estimated from pixels with saliency value higher than the 95% quantile of the image’s saliency distribution. On the other hand, the latter is estimated from pixels with saliency smaller than 30% quantile.

The work evaluates its outputs on test split of the data set for the localization task in the ILSVRC-2013 [31] challenge, where it achieves 46.4% top-5 error in spite of its simplicity. In hindsight, apart from the strategy used to reverse the ReLU layer this approach is equivalent to Deconvnet [23].

3.2.4 Guided Backpropagation

Springenberg et al. proposed a new variant of the deconvolution approach in their work, as a means to analyze their “All Convolutional Net” architecture, which replaces max-pooling layers by convolutional layers with increased stride. The first objective of this work was to empirically prove the equivalence (in terms of predictive performance) between a max-pooling layer and a convolutional layer with an increased stride. This was achieved by evaluating a custom cnn model with max-pooling layers against its convolutional counterpart on three datasets: CIFAR-10, CIFAR-100 and ILSVRC 2012. In all cases, performances of the all convolutional models were on par with their max pooling counterparts. The second objective was to determine the quality of representations learned by the intermediate layers of the all convolutional neural network models. In order to achieve this, authors proposed a visualization approach, which can be considered as a slight modification of the Deconvnet [23] technique.

Back propagation through ReLU

One of the most significant difference between Saliency Maps [30], Deconvnet [23] and Guided backprop [25] approaches is the strategy used by these methods to backpropagate gradients through the ReLU layer.

- Saliency maps approach backpropagates gradients of positions with respective to non-negative activations.
- On the other hand, the deconvnet approach allows only positive gradients to flow in reverse direction.
- The guided-backprop approach combines the above mentioned methods and masks out values for which at least one of activation or gradient values is negative. This is performed with an intention to avoid the reverse of negative gradients of neurons which reduce the activation of the target neuronal unit.

Figure b illustrates differences between back propagation strategies with help of an example feature map.

The term “guided backpropagation” comes from the use of the additional navigation signal, to selectively back propagate only the positive gradients of the positively activated neuronal units. Though guided

backprop was devised to show the learning capability of the all convolutional network architectures, authors show the effectiveness of the technique on the ones with max-pooling units. Guided backprop produced significantly more accurate representation, especially for higher layers, when compared to Deconvnet and Saliency maps.

3.2.5 Deep LIFT

Shrikumar et al. propose an attribution technique, which assigns scores to input pixels based on their contribution to change in activation of each neuronal unit with respect to a reference value, which is chosen based on the problem in hand. Authors claim the technique to be computationally inexpensive, and yield meaningful representations in comparison with other methods. Besides, the technique is devised in a way that it is suitable for neural net variants apart from CNN like Recurrent Neural Networks (RNN). Intuitively, Deep LIFT seeks to explain the deviation in output from some reference output in terms of deviation in input from its respective reference. The motivation to use a reference value, arises from the need to handle the “saturation problem”.

Saturation problem

The saturation problem can be explained intuitively with an example. The figure illustrates a simple neural network whose outputs saturates, when the sum of its inputs (i_1 and i_2) exceeds 1. Application of any perturbation or gradient based attribution method, to this scenario would lead to creation of undesirable artifacts. For the methods of earlier type, perturbing inputs will not cause any changes in the output. On the other hand, gradient based methods will suffer from lack of gradients in the region where $i_1 + i_2 > 1$.

Working

Deep LIFT handles this problem by using a reference value, enabling it to backpropagate the importance signal even in zero and discontinuous gradient situations.

The contributions computed by DeepLIFT is analogous to the idea of partial derivatives, except for the fact that change in input is computed with respect to a finite value (activation difference) in the earlier, in contrast to an infinitesimal value in the latter. The concept of “multipliers” is used to achieve the same. x is the input neuron with a difference from reference Δx , and t is the target neuron with a difference from reference Δt . C is then the contribution of Δx to Δt . Multipliers obey chain rule Along with the custom chain rule, the paper also defines a set of rules for neurons of every kind of neural network layer, to assign contribution scores their inputs:

- Linear rule for linear layers such as the fully-connected and convolutions
- Rescale rule for non-linear transformations such as ReLU, tanh or sigmoid
- Reveal-cancel rule which enables the measurement of marginal effect of having an input over all possible orderings, similar to Shapely values [33].

The technique also takes into account that a zero contribution could be due to cancellation of positive and negative contributions from a pair of entities. The application of DeepLIFT also depends on the choice of target neuron's layer, logit or softmax layer in a classifier network, for example. Authors demonstrate the approach by applying it to a CNN trained on MNIST dataset [34] and an RNN trained on simulated genomic data.

The benchmarking on MNIST classifier for various methods was performed on basis of the change in log-odds score, when a selected pixels of a given image belonging to class c_0 were erased to convert it to an image of some target class c_t . The upper section of figure illustrates the result of masking pixels ordered as the most significant for converting to target classes 3 and 6. As graphically represented in bottom part of figure, DeepLIFT outperformed other backpropagation based methods.

3.3 Layer-wise Relevance Propagation

3.4 Layer Attribution Methods

Layer attribution methods evaluate contribution of each neuronal unit in a given convolutional layer to a model's output. This section discusses three SOTA methods of the category, considered for our work.

3.4.1 GradCAM

Selvaraju et al. propose GradCAM [35], a pixel-attribution technique leveraging the gradients of a given target class with respect to a convolution layer. This approach can be considered as a generalization of CAM for CNNs with fully connected layers. Besides, the technique is applicable to neural network architectures for tasks such as image captioning and visual-question answering. The work also comes up with a means to convert class-agnostic fine grained visualization approaches like Guided-Backprop and Deconvolution to be class-discriminative in nature.

Grad-CAM is one of the most widely used approaches in obtaining attribution map based explanations, for neural network models used with medical data. Concisely put, Grad-CAM creates a visualization of which parts of an input image a convolutional layer “looks” for a certain class prediction. The working of Grad-CAM can be described in the following steps:

1. Perform a forward pass of the input image through CNN to obtain logit scores for all classes.
2. Except for the logit activation of the class of interest, set other activations to zero.
3. Backpropagate the gradient of the class of interest all the way to the chosen convolutional layer containing k feature maps A_k . $\partial y_c / \partial A_k$
4. Global pooling: For every feature map, weigh their pixels based on the gradient value, and obtain their weighted mean value scaled by constant Z where y_c refers to logit score for class c , A^k refers to the k^{th} activation map of dimensions $i \times j$ and α refers to the computed weightage.

5. Obtain the α weighted average of all pooled feature maps and apply a ReLU to filter out negative values, if any present. where L_c refers to the localization map produced by the Grad-CAM for the class of interest c and A_k refers to the k th feature map.
6. An element-wise multiplication operation is applied on the scaled version (input image dimensions) of Grad-CAM's maps, and outputs of fine-grained visualization approaches like Guided-Backpropagation and Deconvolution, to obtain fine-grained yet class discriminative visualizations. These combinations are termed as Guided-GradCAM and Guided-Deconvolution approaches respectively. Guided Grad-CAM visualizations are both high-resolution and class-discriminative.

Typically, last convolutional layers of a neural network model are chosen for Grad-CAM as they contain high-level semantics and detailed spatial information [35]. This is because the attribution maps produced by the methods becomes progressively worse qualitatively, as we use earlier convolutional layers which have relatively lesser receptive fields. In a classification network, logit scores of the target class are used for gradient computations. However, any differentiable activation value can be backpropagated. The embedding based Grad-CAM discussed in the section, draws motivation from this fact. In the original implementation of the attribution method, a Rectified Linear Unit (ReLU) function is applied on heat maps, to obtain only regions that positively affect the given prediction. However, to get better insights into prediction decisions, this work uses unfiltered heat maps, which consists of negatively correlated regions as well.

Authors evaluate the method on three different tasks: weakly-supervised localization, weakly-supervised segmentation and pointing game experiment [36]. The approach is also evaluated and benchmarked on its ability to generate discriminative, trust-worthy, faithful and interpretable attribution maps. A couple of neural network models with different architectures (AlexNet [26] and VGG-16) are used for evaluation, to determine the method's performance consistency across architectures. Finally, the work also demonstrates the association of a given concept with a neuron, similar to the ones presented in [23] and [37].

Authors also demonstrate it use in analyzing failure modes in neural network models and identifying bias in dataset. The approach is considered to be computationally in-expensive when compared to perturbation based methods such as Local Interpretable Model-agnostic Explanations (LIME) [38] or SHapley Additive exPlanations (SHAP) [39], yet producing interpretable and discriminative attribution maps.

3.4.2 HiResolution Class Activation Mapping (HiResCAM)

Draelos et. al propose HiResCAM [40] as a generalization of CAM, and the method aims to use feature maps of a layer directly for visualization without averaging unlike GradCAM. The authors demonstrate why the gradient averaging step in attribution methods like GradCAM limit them from being reliable to highlight a neural network model's regions of attention in an image. Besides, they mathematically show the conceptual relationship between HiResCAM and other CAM approaches. The faithfulness of explanations produced by HiResCAM is shown, by conducting certain experiments on natural images whose results were verified using crowd-sourced assessment.

HiResCAM can be seen as a modification of Grad-CAM, as it is primarily designed to address the

later's limitation caused by its averaging step. As described in 3.4.1 and illustrated in the figure below, importance weight α^f for a feature map f , is computed by computing the mean of gradients over spatial dimensions. However, the process of averaging may cause the final attribution map not highlight locations within the image which the model used to make predictions.

The above figure illustrates the working of GradCAM and HiResCAM methods. Let s_m be the logit score of a CNN model for a given image input, with respect to class m . GradCAM computes the derivative $\partial s_m / \partial A$, which yields the gradient for every position of a feature map. The gradients are then averaged to yield α_m^f for every map. Following which, the gradient values are multiplied with feature activation values ($\alpha_m^f A^f$). While HiResCAM also computes $\partial s_m / \partial A$, they are multiplied directly with feature map activation values leaving out the averaging procedure. Feature map values across channels are then combined as sum to yield the chosen layer's attribution map. By skipping the averaging procedure, HiResCAM preserves the effect of the gradients across every feature map.

Similar to GradCAM, authors recommend using the last convolutional layers for visualization. Apart from proposing the method, the authors also argue that explaining a model doesn't correspond to weakly-supervised segmentation, as the objective of the former to reveal the working of the model while the latter is to localize an object of interest. The work reiterates the fact that every explanation method aims to describe different aspects of model. They also suggest the usage of metrics like IOU to evaluate the localization capability of neural network model than leveraging them to evaluate the correctness of an explanation method. HiResCAM aims to produce faithful explanations even if a model's regions of interest lie outside an object of interest.

The work compares its method with GradCAM by conducting experiments on PASCAL VOC 2012 [29] and a custom made dataset of 20 classes with their ground-truth segmentation maps. Results of the benchmarking experiments reveal the following:

- HiResCAM better reflects computations of the model than GradCAM
- Humans perceive explanations produced by both the methods differently

3.4.3 Full-Grad

Full-grad [41] is a gradient-based attribution method, which produces saliency map explanations by providing attributions to both the input image and the neuronal units of intermediate layers of a given neural network. The method is layer-agnostic and produces a single attribution map for an input image passed through a network by model, considering different scales of features, starting from pixel-level to high-level features. This makes the method to produce sharper saliency maps than other techniques.

Throughout the work, the authors emphasize the importance of a saliency map based explainability method to satisfy two key properties:

1. Completeness: The ability of a saliency map $S(x)$ representation for an input x , to fully encode the computation performed by a function $f(x)$, such that it can be recovered using $S(x)$ and x .

2. Weak dependence: In a piece-wise linear model, $S(x)$ is dependent only on local neighborhood of x in the data space.

Authors claim that other saliency mapping methods are able to satisfy only either of these properties. This inability arises from the exclusion of gradient contributions from the bias components of a neural network model. Besides, they also stress on the need for a saliency mapping method to attribute importance to individual (local attribution) and regions of pixels (global attribution) simultaneously. The novelty of this work lies in its ability to simultaneously satisfy both the completeness and weak dependence properties, by considering gradients associated with bias components for producing saliency maps.

The following equation expresses the idea that a ReLU neural network with bias b can be approximated as the sum of input gradients and bias gradients. The bias term b here considers both explicit bias component and implicit bias such as running mean of batch normalization layers.

Figure shows the ability of the Full-grad method to produce meaningful saliency maps by accumulating both bias and input gradients across all hidden layers. The work also provides the rationale behind its ability to be sensitive to saturation scenarios like zero input attribution, and to produce in correct input-output mappings in the case of parameter randomization. The method first obtains spatial maps (R^D) for every convolutional filter called neuron-wise maps. Such maps are then aggregated to form layer-wise maps. The layer-wise maps are further processed by rescaling supplemented with an absolute value operation. The following equation mathematically expresses the process:

The authors evaluate the effectiveness of the method by conducting two quantitative experiments:

1. Pixel perturbation: Replace the least salient input pixels for classification with black pixels, and observe the output variation. The lower the variation in salient regions of the attribution maps, the better is a method.
2. RemOve And Retrain (ROAR) experiment [42]: In this experiment, the top-k pixels highlighted by an attribution method for an entire data set are removed, and the considered classifier is retrained on this modified data set. The attribution method corresponding to the least accurate classifier model is considered to be the best, as it indicates that the method correctly identified the salient pixels.

The work reports that the FullGrad method outperformed the other considered methods (Input-gradients [43], Integrated-gradients [44], Smooth Grad [45] and GradCAM [35]) in both the experiments. Apart from the quantitative evaluation, the authors also conducted a visual inspection in which they found the method to produce meaningful attribution maps which highlight both a given object's boundaries and interiors clearly. Figure

4

Methodology

Last chapter gave a literature review of different attribution methods available to explain neural network models like GestaltMatcher. This chapter explains the methodical approach taken to address the research problem at hand, by discussing the design of experiments and rationale behind different choices made to conduct them.

4.1 Datasets

This research work uses two datasets for conducting experiments. Frontal facial images of patients with rare genetic syndrome are taken from the GestaltMatcher DataBase (GMDB) dataset. The dataset contains 12849 facial images from 7640 patients with 742 different syndromes. Besides patient images, the dataset also contains other details such as patient history. GMDB acts a valuable resource for the research community.

The UTKFace [46] is used for the dataset imbalance - explanation quality experiment 4.3 that requires faces from a healthy cohort. The dataset has over 20,000 face images with labels for age, gender and ethnicity. For the experiment, we handpick 244 samples from the dataset, while ensuring the diversity of the dataset.

4.2 Selection of Methods

In this section, we analyze the neural network explainability methods discussed in Chapter 2 based on the following dimensions and identify the ones to be considered for further experimentation and evaluation:

- **Saturation problem:** As briefly described in 3.2.5, saturation problem occurs when the output of a neural network model gets saturated and its gradients with respect to inputs become insensitive, thereby affecting the quality of generated attribution maps. Shrikumar et al. [43] reported that occlusion sensitivity maps, layer-wise relevance propagation, saliency maps, guided-backpropagation and guided-GradCAM methods suffer from this problem. Besides, they also report the failure of deconvolution approach in the presence of discontinuous input gradients.
- **Sensitivity to changes in model and data:** Adebayo et al. [47] investigated faithfulness of explanations produced by popular attribution methods. The chosen methods were evaluated based on their sensitivity to randomization induced in the considered neural network model's weights and

labels of the training instances. Authors report that guided-backpropagation and guided-GradCAM remained insensitive to the changes in model and data, having functioned merely as edge detectors. GradCAM passed this sanity check.

- **Robustness of explanations:** An interpretability method is robust when it generate similar explanations for similar inputs. David Alvarez et al. [48] and Yi-han Sheu [49] reported that DeepLIFT experiences robustness issues and produces inaccurate results in the presence of multiplicative interactions between features. Besides the lack of robustness, the success of DeepLIFT depends on factors such the choice of reference/baseline image, which is difficult to determine.
- **Relevance to the problem at hand:** Along with the above list dimensions, this work shortlists the methods based on their ability to produce meaningful explanations in the context of genetic syndrome recognition. Figures 4.1 and 4.2 shows few sample attribution maps generated from applying both the considered sets of input and layer attribution maps to the GestaltMatcher model. It can be observed that contours of regions in attribution maps produced by layer attribution methods closely match the scales of phenotypic features of genetic syndromes and parts of human face, in general. This effect is possibly due to the inherent working principles of the two classes of attribution methods.

Layer attribution maps are obtained by scaling and superimposing feature map activations of the last convolutional layers of a CNN, which are responsible for extracting high-level features from a given input image. This nature makes them more suitable for the problem at hand than input attribution methods, which represent pixel-wise attribution methods.

4.2.1 More Reasons to Consider Layer Attribution Methods

In addition to the above discussed reasons, it is also observed that layer attribution approaches like GradCAM are widely used to explain neural network models for medical diagnosis [1] [2]. However, the downside of GradCAM is it approaches attribution as weakly supervised segmenation problem and “sometimes higlight locations the model didnot actually use” [40]. HiResCAM [40], a recent successor of GradCAM overcomes this issue and produces more faithfulness explanations. Therefore, the method is included in the scope of this work.

GradCAM and HiResCAM are layer-specific and therefore their explanations are limited by the choice of the convolutional layers made. FullGrad [41] overcomes this deficit by considering attributions across all neuronal units of a model and thus becomes a candidate for experimentation. Along with these CAM techniques, occlusion sensitivity mapping is included as a reference explanation method, to better understand the classifier model’s regions of attention.

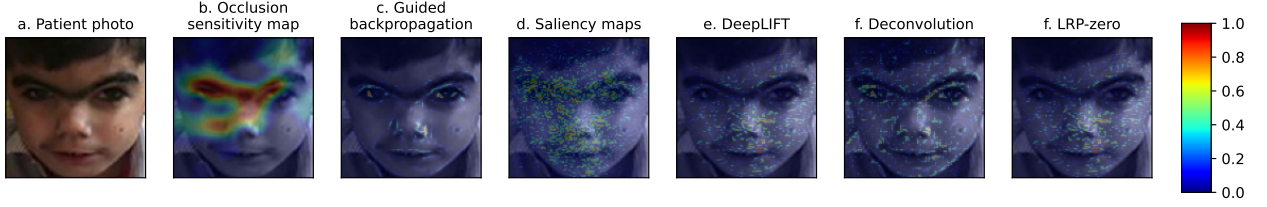


Figure 4.1: An example showing input attribution maps of discussed methods, generated for a patient image

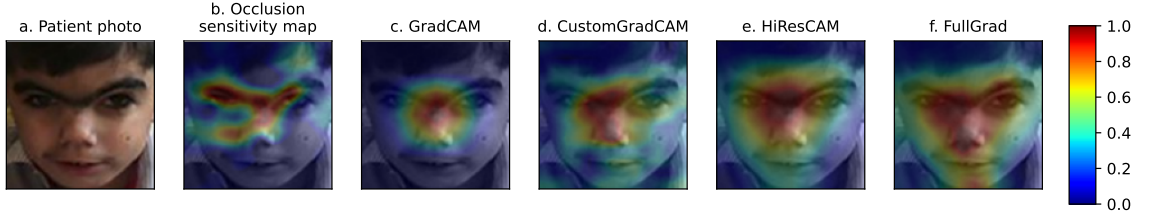


Figure 4.2: An example for layer attribution maps of discussed methods, generated for a patient image

4.3 Design of Experiments

Figure 4.3 illustrates the methodical approach taken to realize the objectives of this research work. The previous chapter and Section 4.2 discussed the XAI methods considered for this work and explained the rationale to select three of them for further experimentation. The next step is to integrate the selected set of methods with the GestaltMatcher model, on which the planned experiments are conducted.

A. Patient-wise Attribution Maps Generation

This experiment focuses on one of our research objectives, to use XAI methods to generate explanations for individual predictions produced by the GestaltMatcher model. Patient-wise attribution maps help us in knowing GestaltMatcher's attention regions in every patient face from GMDB dataset. In turn, this helps us to study the patterns (if there is any) behind the model's varying regions of interests for different categories of inputs.

B. Composite Face Generation

Experiments B and C are conducted with an intent to obtain a characteristic representation of GestaltMatcher's regions of interest in a syndrome(class)-wise manner. Composite face representation of a given class is obtained by applying certain image transformations and averaging patient faces belonging to it (see ?? Chapter 5 for the detailed description). Thus generated composite faces are then processed by the XAI integrated GestaltMatcher model to produce its corresponding attribution maps using all three selected methods.

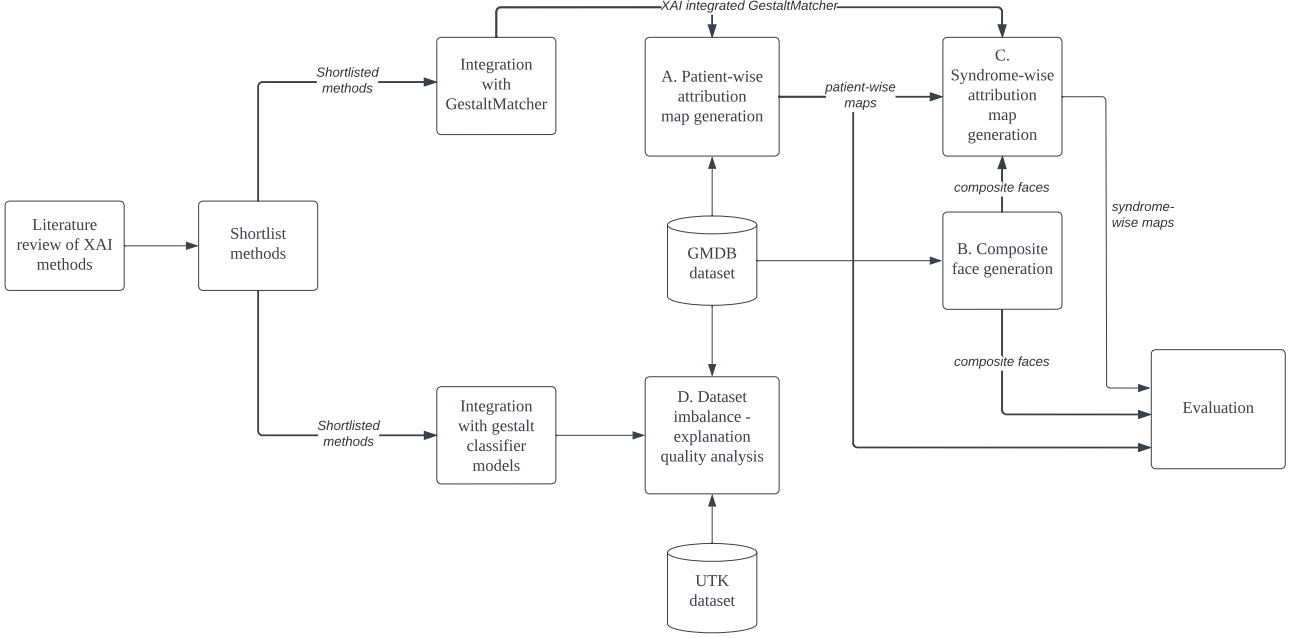


Figure 4.3: Design of experiments

C. Syndrome-wise Attribution Maps Generation

Although, attribution maps of composite faces are generated with an intent to give a generic representation, they suffer from a couple of drawbacks. The process of applying image transformations to facial images of patients to generate composite faces, may alter the key facial abnormalities and dysmorphic features associated with corresponding genetic syndromes. Besides, there is a possibility of the GestaltMatcher model to misclassify them, raising concerns about the correctness of generated attribution maps.

In order to overcome these challenges, we propose and deploy two other techniques to produce syndrome-wise attribution maps: averaging and Singular Value Decomposition (SVD). These techniques are applied to only attribution maps associated with correctly predicted inputs. However, syndrome-wise attribution maps generated using all the three techniques are considered for evaluation, provided the composite face of a given syndrome is correctly predicted.

D. Dataset Imbalance - Explanation Quality Analysis

As discussed in Section 1.3, GMDB dataset is imbalanced. We hypothesize that the problem could affect the quality of attribution maps generated from the GestaltMatcher model. This experiment verifies the hypothesis.

We train three different classifier models: two trained with balanced sets of classes, and one with an

imbalanced set. We observe and analyze the changes in attribution maps produced from these models. Besides this investigation, we study the variations in GestaltMatcher’s regions of attention in syndromic and healthy faces. This is realized by analyzing attribution maps produced from a binary classifier, which is trained to differentiate faces of syndromic and healthy individuals. Facial images of healthy people are obtained from the UTKFace dataset.

4.4 Evaluation

Evaluating XAI methods based on their explanation correctness remains a challenge till date. Yeh *et al.* [50] classifies explanation evaluation measures into two categories: objective or computational measures and subjective measures. Objective measures evaluate explanations based on whether a given XAI method satisfies certain properties or axioms, such as completeness [44]. On the other hand, subjective measures focus on aspects such as explanation usefulness, and the evaluation procedure involves humans. This research work uses subjective measures to evaluate the explanation artifacts produced by the chosen set of XAI methods.

In the beginning, this section briefly explains the two predominantly used objective measures to evaluate saliency mapping methods: “infidelity and sensitivity” [50], to give the reader an idea about what computational metrics typically look for. Subsequently, the rationale behind using subjective measures over objective ones for this work is provided. Finally, the proposed evaluation procedure is described in detail.

4.4.1 Objective Measures

Yeh *et al.* [50] proposed infidelity and sensitivity metrics in their work, to benchmark various saliency mapping methods. These measures are computed based on the changes observed in model explanations, when its inputs are subject to perturbations.

Infidelity

$$\text{content...} \quad (4.1)$$

Infidelity computes the expected mean squared difference between an explanation scaled by the magnitude of an input perturbation, and differences between the predictor function of the given model at its input and perturbed input. Intuitively, this refers to the correctness of an XAI method in generating true explanations for model predictions.

Sensitivity

$$\text{content...} \quad (4.2)$$

Sensitivity can explained as the change in model explanation resulting from a small perturbation in the input.

4.4.2 Rationale to Adopt Subjective Evaluation

Although, computational measures such as the ones presented offer a quantitative means to benchmark XAI methods, they cannot be used for evaluating them on abstract objectives such as meaningfulness of explanations. Such an evaluation can only be performed in subjective manner, by end users of the AI system.

Mohseni *et al.* [51] list various possible goals with which XAI methods can be used, and also recommend measures to evaluate them, based on the context of their application. The goals listed in their work are as follows: algorithmic transparency, user trust and reliance, bias mitigation, privacy awareness, model visualization and inspection, model tuning and selection, model interpretability and debugging.

The primary goals of this research work can be related to three of the above mentioned: “algorithmic transparency”, “user-trust and reliance” and “model interpretability”. For such cases, authors recommend to evaluate XAI methods by conduct human-subject studies using tools such as Likert-scale questionnaires [52]. This research work follows the recommendation, and formulates a questionnaire for clinicians (end-users) to evaluate the generated explanations.

4.4.3 Proposed Evaluation Procedure

The three types of artifacts (patient-wise map, composite face and syndrome-wise map) generated from the above mentioned experiments are meant to be evaluated by clinicians, who are familiar with the syndromes in our scope. This research work formulates evaluation procedures for each artifact. Clinical practitioners were consulted to develop the procedures. The proposed evaluation strategies are realized in the form of a questionnaire, which is presented in ?? Chapter 5.

i. Patient-wise Attribution Maps

Steps to evaluate patient-wise maps are presented in Figure 4.4 as a flowchart. Besides illustrating the process flow, the chart enumerates possible responses and what can be inferred from them. Scenarios B and C are desirable, as they indicate the usefulness of attribution maps. The final step ranks attribution maps generated by the four chosen methods based on their usefulness.

It is important to note that this evaluation procedure is performed on attribution maps of correctly predicted test samples from GMDB dataset. The idea to evaluate attribution maps of test instances is based on the recommendation from Molnar in his book titled “Interpretable Machine Learning” [53].

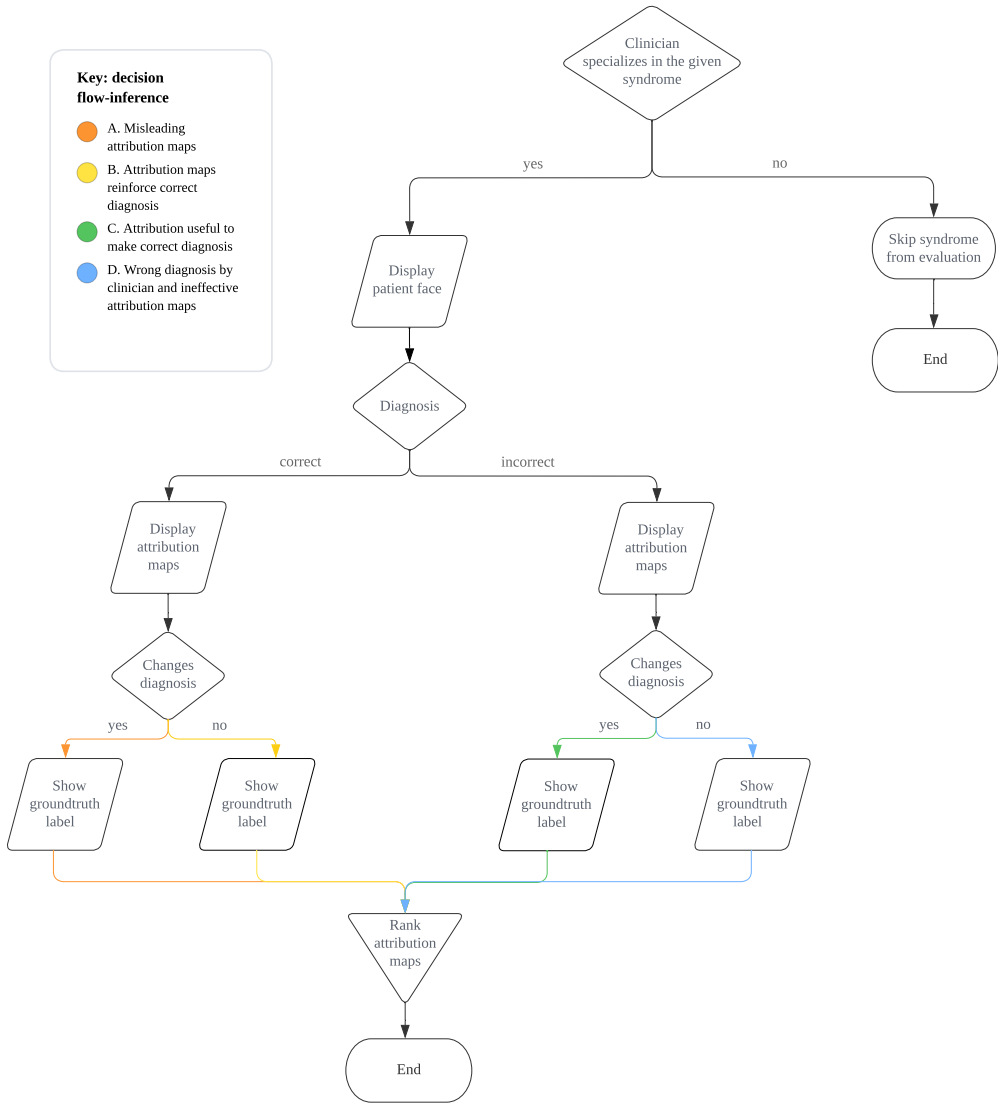


Figure 4.4: Proposed procedure to evaluate patient-wise attribution maps

ii. Composite Faces

The implicit goal of evaluating composite faces is to know if they contain all or most of characteristic facial features of a genetic syndrome. Unlike the case of individual patient images, ground truth labels associated with composite faces are not known before hand, as they are synthesized using facial features from multiple images of a class. Therefore, at first it is important to know whether a given composite face atleast resembles a patient face of a particular syndrome, before looking for its prominent features. The same idea is illustrated as a flowchart in Figure 4.6.

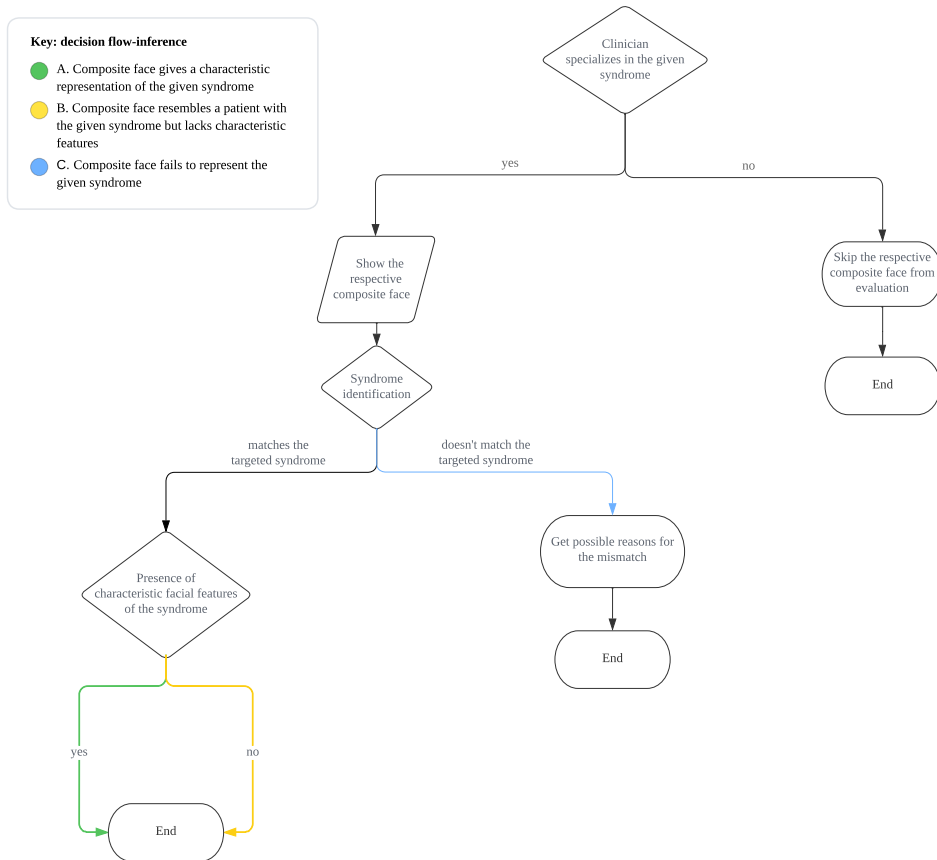


Figure 4.5: Proposed procedure to evaluate composite faces

iii. Syndrome-wise Attribution Maps

Syndrome-wise attribution maps are evaluated in a single step process. The target syndrome is revealed, and the evaluator is asked to pick top three attribution maps, based on how well they highlight the facial regions containing all or most of the disorder's features.

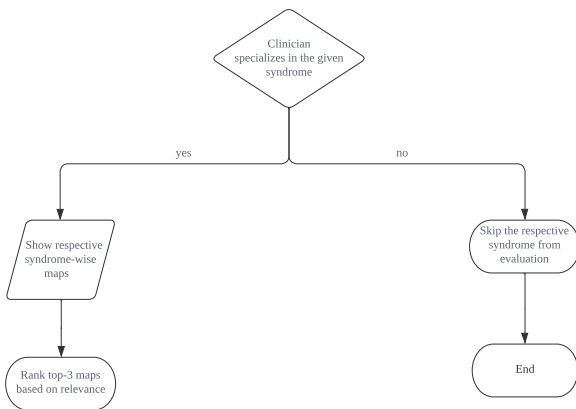


Figure 4.6: Proposed procedure to evaluate composite faces

5

Implementation

This chapter describes gives implementation details of the experiments conducted during this thesis work. In the beginning architectural specifications of GestaltMatcher are provided. Subsequently, we describe the procedure to integrate explanation methods with the model. Furthermore, implementation details of the experiments proposed in the previous chapter are discussed. Finally, the evaluation questionnaire is presented.

5.1 GestaltMatcher Architecture

The procedure to diagnose rare-genetic syndromes from patient faces using GestaltMatcher is described in a detailed manner in Chapter 2 ???. This section describes the architecture of its underlying Convolutional Neural Network (CNN) backbone and steps involved in preprocessing its input images. The pipeline shown in Figure 5.6 illustrates the sequence of steps involved in processing a patient photo using GestaltMatcher.

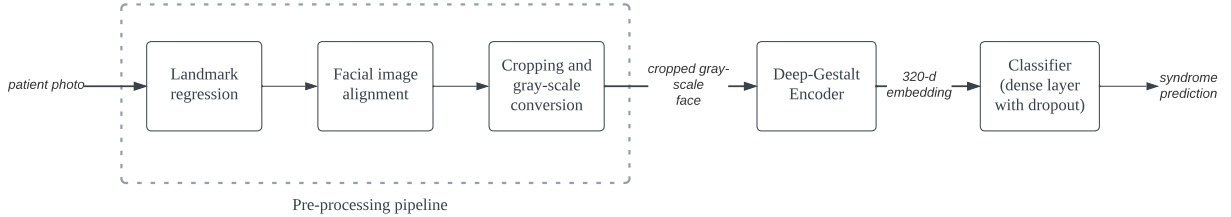


Figure 5.1: Illustration of the pipeline to process a patient photo using GestaltMatcher

Pre-processing Pipeline

The pre-processing pipeline is responsible for detecting facial landmarks and aligning the orientation of a given patient photo, and finally cropping the face from it. Authors of GestaltMatcher use RetinaFace [54] to fetch detect landmark points from a patient's facial image. In a nutshell, RetinaFace is a single-stage, multi-scale face localization method which employs multi-task learning to perform five different tasks:

5.2. Explanation Methods - GestaltMatcher Integration

face detection, landmark position and score regression, 3D position and pixel correspondence prediction. It uses a Resnet-50 [55] backbone. The facial landmark coordinates outputted by RetinaFace is used to crop and align faces from patient photos. The facial images are resized to 100 x 100, and converted to gray-scale before feeding them to the GestaltMatcher neural network model.

Architecture Specifications

GestaltMatcher consists of an encoder and a classifier module. The encoder is called as "Deep Gestalt encoder", named after the work [10] in which its architecture was first proposed. Deep Gestalt encoder uses a CNN to extract discriminative features from input facial images, and represent them in 320-dimensional embedding space called the "Clinical Face Phenotype Space" (CFPS). As explained in Chapter 2??, an embedding projected onto the CFPS can be used to match its corresponding patient photo to a gallery of facial portraits of unsolved or solved cases. For syndrome recognition, a fully-connected layer, which acts as classifier, is appended to the encoder.

Model Training

The presented neural network is first trained on facial images from the CASIA-WebFace [56] dataset. Subsequently, it is trained on 139 frequent-syndrome classes listed in the GestaltMatcher paper [15]. The training details are presented in ??.

5.2 Explanation Methods - GestaltMatcher Integration

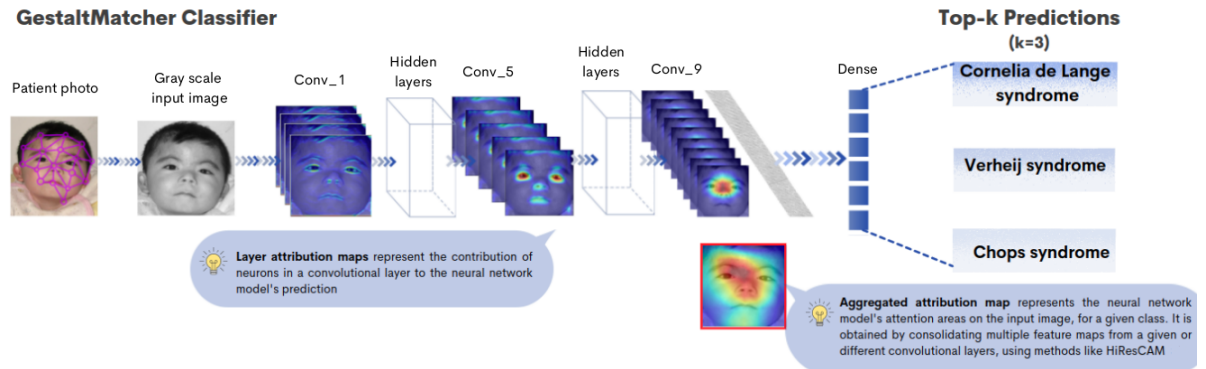


Figure 5.3: An illustration of attribution map computation from the GestaltMatcher model

The Class Activation Mapping (CAM) methods used for this work typically generate class-specific attribution maps, by evaluating contributions of neurons in a given convolutional layer to the model output. Therefore, the choice of target convolutional layer plays a vital role. Selvaraju *et al.* [35] recommend to use the last convolutional layers, as they contain more high-level semantic and spatial information, when compared to earlier layers, which have smaller receptive fields. The same is reinforced by Muhammad *et al.* [57]. We validated this recommendation by computing and comparing attribution maps generated from

Layer (type)	Input Shape [channels, rows, columns]	Output Shape [channels, rows, columns]	Kernel Shape [count, channels, rows, columns]
1. Conv_Norm_Act	[1, 100, 100]	[32, 100, 100]	--
a. Conv2d	[1, 100, 100]	[32, 100, 100]	[1, 32, 3, 3]
b. BatchNorm2d	[32, 100, 100]	[32, 100, 100]	[32]
c. ReLU	[32, 100, 100]	[32, 100, 100]	--
2. Conv_Norm_Act	[32, 100, 100]	[64, 100, 100]	--
a. Conv2d	[32, 100, 100]	[64, 100, 100]	[32, 64, 3, 3]
b. BatchNorm2d	[64, 100, 100]	[64, 100, 100]	[64]
c. ReLU	[64, 100, 100]	[64, 100, 100]	--
3. MaxPool2d	[64, 100, 100]	[64, 50, 50]	--
4. Conv_Norm_Act	[64, 50, 50]	[64, 50, 50]	--
a. Conv2d	[64, 50, 50]	[64, 50, 50]	[64, 64, 3, 3]
b. BatchNorm2d	[64, 50, 50]	[64, 50, 50]	[64]
c. ReLU	[64, 50, 50]	[64, 50, 50]	--
5. Conv_Norm_Act	[64, 50, 50]	[128, 50, 50]	--
a. Conv2d	[64, 50, 50]	[128, 50, 50]	[64, 128, 3, 3]
b. BatchNorm2d	[128, 50, 50]	[128, 50, 50]	[128]
c. ReLU	[128, 50, 50]	[128, 50, 50]	--
6. MaxPool2d	[128, 50, 50]	[128, 25, 25]	--
7. Conv_Norm_Act	[128, 25, 25]	[96, 25, 25]	--
a. Conv2d	[128, 25, 25]	[96, 25, 25]	[128, 96, 3, 3]
b. BatchNorm2d	[96, 25, 25]	[96, 25, 25]	[96]
c. ReLU	[96, 25, 25]	[96, 25, 25]	--
8. Conv_Norm_Act	[96, 25, 25]	[192, 25, 25]	--
a. Conv2d	[96, 25, 25]	[192, 25, 25]	[96, 192, 3, 3]
b. BatchNorm2d	[192, 25, 25]	[192, 25, 25]	[192]
c. ReLU	[192, 25, 25]	[192, 25, 25]	--
9. MaxPool2d	[192, 25, 25]	[192, 13, 13]	--
10. Conv_Norm_Act	[192, 13, 13]	[128, 13, 13]	--
a. Conv2d	[192, 13, 13]	[128, 13, 13]	[192, 128, 3, 3]
b. BatchNorm2d	[128, 13, 13]	[128, 13, 13]	[128]
c. ReLU	[128, 13, 13]	[128, 13, 13]	--
11. Conv_Norm_Act	[128, 13, 13]	[256, 13, 13]	--
a. Conv2d	[128, 13, 13]	[256, 13, 13]	[128, 256, 3, 3]
b. BatchNorm2d	[256, 13, 13]	[256, 13, 13]	[256]
c. ReLU	[256, 13, 13]	[256, 13, 13]	--
12. MaxPool2d	[256, 13, 13]	[256, 7, 7]	--
13. Conv_Norm_Act	[256, 7, 7]	[160, 7, 7]	--
a. Conv2d	[256, 7, 7]	[160, 7, 7]	[256, 160, 3, 3]
b. BatchNorm2d	[160, 7, 7]	[160, 7, 7]	[160]
c. ReLU	[160, 7, 7]	[160, 7, 7]	--
14. Conv2d	[160, 7, 7]	[320, 7, 7]	[160, 320, 3, 3]
15. AvgPool2d	[320, 7, 7]	[320, 1, 1]	--
16. Dropout	[320]	[320]	--
17. Linear	[320]	[139]	[320, 139]

Figure 5.2: Architecture of the CNN in GestaltMatcher. The convolution layer 14 used to generate attribution maps using GradCAM and HiResCAM methods is highlighted using a blue box. Layers (10.a, 11.a and 14) that are used by the CustomGradCAM method are highlighted using cyan boxes.

all ten convolutional layers, using both GradCAM and HiResCAM techniques. FullGrad was excluded from this analysis, as the method is layer-agnostic in nature. Based on the recommendation and our observations, we chose layer 14 (refer conv_9 in Figure 5.4), the last convolutional layer to compute attribution maps.

CustomGradCAM

Apart from the last convolution layer, we also observed that applying GradCAM to layers 10.a and 11.a produced visualizations in which certain key features of human face are highlighted (refer conv_6 and conv_7 in Figure 5.4). Therefore, in order to include the layers in our scope, we averaged their attribution maps along with the ones produced by layer 14. The resulting map is presented under the name of

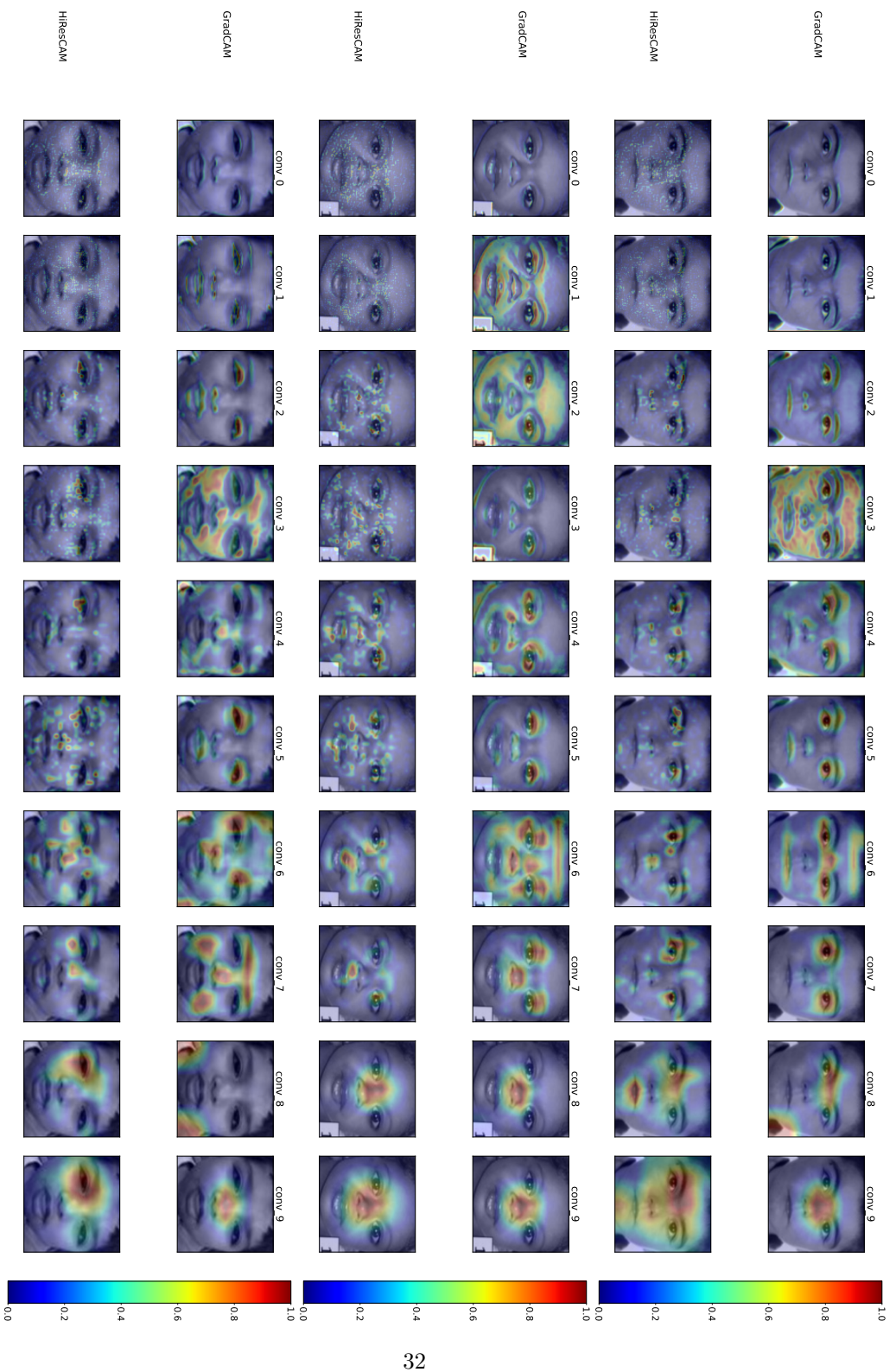


Figure 5.4: Layer-wise visualization of attribution maps generated by GradCAM and HiResCAM methods.

“CustomGradCAM”. We used the Application Programming Interfaces (APIs) offered by PyTorch [61], Captum [22] and an open-source library [60] to integrate the explanation methods to the GestaltMatcher classifier model.

5.2.1 Visualization Details

Captum’s visualizer tool was used to generate color coded attribution maps. We post-processed attribution maps to remove noise and visual artifacts. This section provides details on visualization parameters and the post-processing procedure.

Interpolation

The attribution maps generated by layer-specific methods such as GradCAM and HiResCAM are shaped identical to the feature maps outputted by the target layers. For example, layer 14 of the gestaltmatcher model spits out 320 7x7 (height x width) feature maps, and any attribution map generated from the layer is of dimensions 7x7 (height x width). The bilinear interpolation technique [58] was used to rescale attribution maps to the input image size of 100x100 (height x width), so that the map could be overlaid on the input image.

Attribution Sign and Representation

We considered only positive attribution values for visualization and used the “jet” colormap scheme offered by Captum’s [22] visualization tool.

Smoothing Attribution Maps

Test Time Augmentation (TTA) is a commonly used technique to boost the performance of image classification models [59]. During the inference process for a given input image, instead of passing the actual sample, its augmented counterparts are fed to obtain predictions from the model. Thus obtained predictions are averaged to obtain the final output. Augmented copies are obtained by applying transformations such as rotations and flips to the original input image.

In our work, we used TTA to enhance the quality of generated attribution maps. Augmented copies of every test input image were obtained by individually applying horizontal flipping and multiplications (with factors of 0.9, 1 and 1.1) operations. Attribution maps were generated for each augmented copy, and finally averaged to obtain the smoothed map. Attribution maps produced from HiResCAM were exempted from TTA based on the guidelines provided by Jacob Gildendblat [60].

5.3 Experiments

Implementation details of the conducted set of experiments are presented in this section.

5.3.1 Patient-wise Attribution Map Generation

Patient-wise attribution maps are generated by applying the chosen set of methods to individual patient images. The attributions are computed with respect to the logit scores of the samples' ground truth classes. This is because the attribution "methods work only when the classification result is correct" [57]. However, an experiment was also conducted to observe the differences between explanations of misclassified samples, obtained by computing attributions with respect to their ground truth and predicted labels. Its results are discussed in the next chapter.

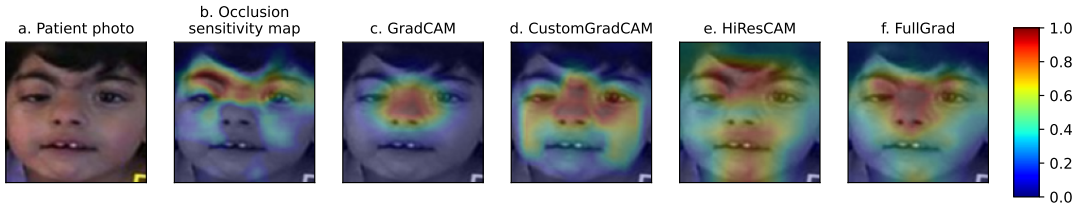


Figure 5.5: An example for patient-wise attribution maps

5.3.2 Composite Face Generation

Composite faces are generated with an intent to synthesize a characteristic face for each genetic syndrome class under our scope. Concisely put, they are obtained from aligning and averaging facial images of each category separately. This section provides a detailed description of the process involved.

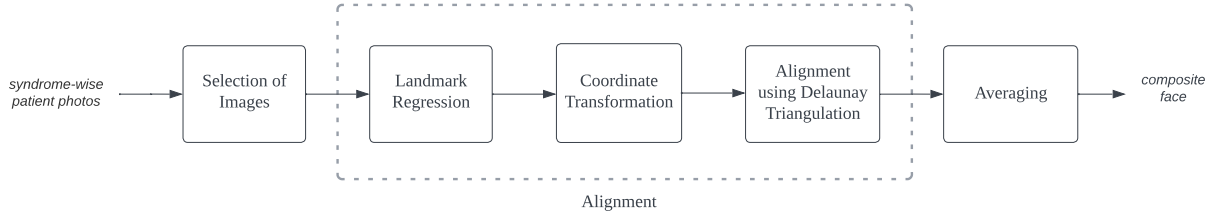


Figure 5.6: Block diagram representing composite face generation process

a. Selection of Images

The first step involved in generating composite faces is to select the right constituent images. A considerable number of images in ?? GMDB are characterized by poor visual quality and/or presence of artifacts. A few such as the ones shown in Figure ?? also contain objects like nasal catheter tubes, spectacles, and black strips which were introduced to conceal patient identities. Therefore, we hand picked images from each of 139 syndrome classes to remove the unsuitable candidates for generating composite faces.

<Bad image examples>

b. Facial Landmark Regression

Landmark points act as anchors to align the constituent images of composite faces. 68 landmark points are calculated for each input facial image using the dlib ¹library's face detector functionality. Internally, dlib uses a CNN based max-margin object detector to perform the task. <Facial landmark example image> <dlib link>

c. Coordinate Transformation

The next step warps the constituent facial images in a such a way that their landmark points corresponding to the right corner of the right eye and the left corner of the left eye are shifted to locations P_1 ($0.3 \times$ image width, $0.3 \times$ image height) and P_2 ($0.7 \times$ image width, $0.3 \times$ image height) respectively. In practice this is achieved by computing and applying a similarity transformation matrix using OpenCV library's "estimateRigidTransform" method.

Similarity transformation [62] is a specialization of projective transformations, composed of an euclidean transformation (rotation and translation), and an isotropic scaling. Planar similarity transformation has four Degrees Of Freedom (DOFs) can be expressed in the following form: <equation>

Planar affine transformation has two more DOFs offered by non-isotropic scaling and shear. A planar affine transformation can represented in the form of following matrix:

d. Facial Alignment using Delaunay Triangulation

Facial images are now anchored at points P_1 and P_2 . However, their regions are yet to be aligned to a common reference. Such a reference is obtained by computing the mean of landmark points of all constituent faces. Subsequently, every facial image is split into regions using Delaunay triangulation technique. "A Delaunay triangulation of a vertex set is a triangulation of the vertex set with the property that no vertex in the vertex set falls in the interior of the circumcircle (circle that passes through all three vertices) of any triangle in the triangulation" [63]. An affine transformation is computed for every triangular region using its vertices, to warp and fit it in the corresponding region formed by the mean landmark points.

e. Averaging

The aligned sets of images are averaged to form their corresponding composite faces.

5.3.3 Syndrome-wise Attribution Map Generation

Syndrome-wise attribution maps are generated using three different methods and their implementation details are discussed below.

¹dlib library - <http://dlib.net/>.

i. Attribution Maps of Composite Faces

The first type of syndrome-wise maps are obtained by treating composite faces as individual patient faces and applying the patient-wise attribution map generation procedure.

ii. Average Attribution Maps

Average attribution map of a given syndrome is obtained by computing the mean across attribution maps of the correctly predicted instances from the class's test split.

iii. Singular Value Decomposition (SVD) of Attribution Maps

Eigen-CAM [57] is a layer attribution technique, which computes saliency from the first principal component of feature activations of channels, across the target convolutional layer. For this experiment, we apply the same technique to the attribution maps of correct predicted samples of a given class, for obtaining its characteristic saliency map. The procedure is described in a step-wise manner below:

1. Vectorize the attribution maps of correctly predicted samples of a given syndrome class c into a matrix A_c .
2. Mean subtraction $\langle \rangle$
3. Factorize A_c using SVD to compute principal components of A_c

$$A_c = U\Sigma V^T \quad (5.1)$$

where U is an $M \times M$ orthogonal matrix and V is an $N \times N$ orthogonal matrix. The columns of U and V form the left and right singular vectors of A_c respectively. The resultant attribution map R_c is obtained by projecting A on the first right eigen vector V_1 :

$$R_c = A_c V_1 \quad (5.2)$$

The procedure is applied individually on attribution maps of all the three GradCAM, HiResCAM and FullGrad methods, for all syndromes under our scope. In the cases of average and SVD of attribution map visualizations, a given syndrome's composite face is used as the background image to project the maps, although there is no relationship between them.

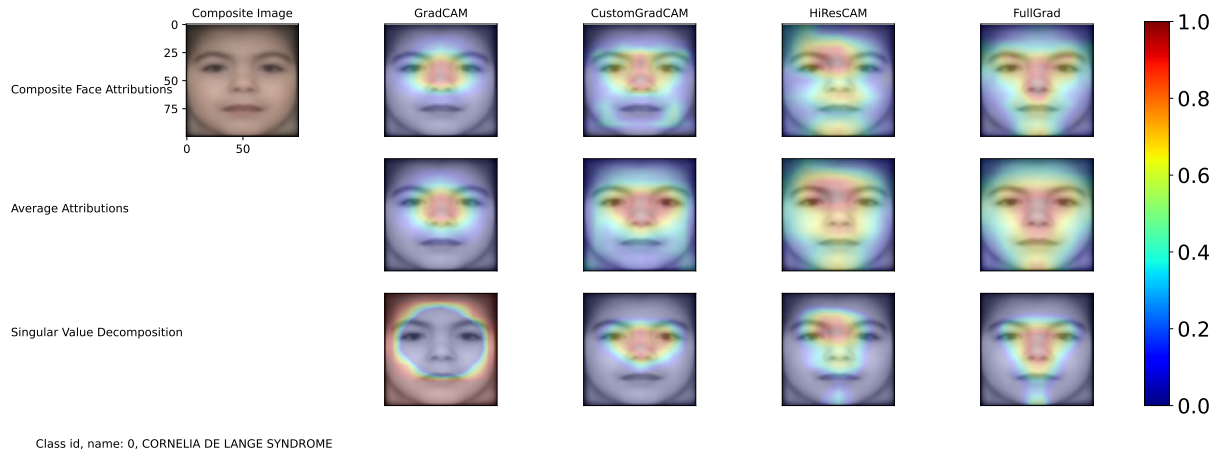


Figure 5.7: An example for syndrome-wise attribution maps

5.3.4 Dataset Imbalance - Explanation Quality Analysis

5.4 Evaluation Questionnaire

6

Evaluation and Results

6.1 Metrics

Describe the experiments/evaluation you are performing to analyse your method.

6.2 Qualitative Analysis

6.2.1 Patient-wise Maps

6.2.2 Syndrome-wise Maps

6.2.3 Composite Faces

6.3 Effect of Class Imbalance on the Explainability of Models

6.4 Quantitative Analysis

6.4.1 Use of Occlusion Sensitivity Maps

6.4.2 Eye-tracking based Evaluation

6.4.3 Similarity Mapping

6.5 Evaluation Summary

Describe the results of your experiments in detail.

7

Conclusions

7.1 Contributions

7.2 Lessons learned

7.3 Future work

A

Design Details

Your first appendix

B

Parameters

Your second chapter appendix

References

- [1] S. M. Anwar, M. Majid, A. Qayyum, M. Awais, M. Alnowami, and M. K. Khan, “Medical image analysis using convolutional neural networks: a review,” *Journal of medical systems*, vol. 42, no. 11, pp. 1–13, 2018.
- [2] T. Ozturk, M. Talo, E. A. Yildirim, U. B. Baloglu, O. Yildirim, and U. R. Acharya, “Automated detection of covid-19 cases using deep neural networks with x-ray images,” *Computers in biology and medicine*, vol. 121, p. 103792, 2020.
- [3] Z. Xue, S. Antani, L. R. Long, D. Demner-Fushman, and G. R. Thoma, “Window classification of brain ct images in biomedical articles,” in *AMIA Annual Symposium Proceedings*, vol. 2012. American Medical Informatics Association, 2012, p. 1023.
- [4] H. Lee, S. Yune, M. Mansouri, M. Kim, S. H. Tajmir, C. E. Guerrier, S. A. Ebert, S. R. Pomerantz, J. M. Romero, S. Kamalian *et al.*, “An explainable deep-learning algorithm for the detection of acute intracranial haemorrhage from small datasets,” *Nature biomedical engineering*, vol. 3, no. 3, pp. 173–182, 2019.
- [5] X. Qian, J. Pei, H. Zheng, X. Xie, L. Yan, H. Zhang, C. Han, X. Gao, H. Zhang, W. Zheng *et al.*, “Prospective assessment of breast cancer risk from multimodal multiview ultrasound images via clinically applicable deep learning,” *Nature biomedical engineering*, vol. 5, no. 6, pp. 522–532, 2021.
- [6] S. A. Hicks, J. L. Isaksen, V. Thambawita, J. Ghose, G. Ahlberg, A. Linneberg, N. Grarup, I. Strümke, C. Ellervik, M. S. Olesen *et al.*, “Explaining deep neural networks for knowledge discovery in electrocardiogram analysis,” *Scientific reports*, vol. 11, no. 1, pp. 1–11, 2021.
- [7] A. Binder, M. Bockmayr, M. Hägele, S. Wienert, D. Heim, K. Hellweg, M. Ishii, A. Stenzinger, A. Hocke, C. Denkert *et al.*, “Morphological and molecular breast cancer profiling through explainable machine learning,” *Nature Machine Intelligence*, vol. 3, no. 4, pp. 355–366, 2021.
- [8] C. Li, D. Konomis, G. Neubig, P. Xie, C. Cheng, and E. Xing, “Convolutional neural networks for medical diagnosis from admission notes,” *arXiv preprint arXiv:1712.02768*, 2017.
- [9] F. Schwendicke, T. Golla, M. Dreher, and J. Krois, “Convolutional neural networks for dental image diagnostics: A scoping review,” *Journal of Dentistry*, vol. 91, p. 103226, 2019. [Online]. Available: <https://www.sciencedirect.com/science/article/pii/S0300571219302283>
- [10] Y. Gurovich, Y. Hanani, O. Bar, G. Nadav, N. Fleischer, D. Gelbman, L. Basel-Salmon, P. M. Krawitz, S. B. Kamphausen, M. Zenker *et al.*, “Identifying facial phenotypes of genetic disorders using deep learning,” *Nature medicine*, vol. 25, no. 1, pp. 60–64, 2019.

-
- [11] S. M. McKinney, M. Sieniek, V. Godbole, J. Godwin, N. Antropova, H. Ashrafi, T. Back, M. Chesus, G. S. Corrado, A. Darzi *et al.*, “International evaluation of an ai system for breast cancer screening,” *Nature*, vol. 577, no. 7788, pp. 89–94, 2020.
 - [12] “Explainable AI,” Mar. 2021, [Online; accessed 4. May 2022]. [Online]. Available: <https://www.ibm.com/watson/explainable-ai>
 - [13] B. Ghoshal and A. Tucker, “Estimating uncertainty and interpretability in deep learning for coronavirus (covid-19) detection,” *arXiv preprint arXiv:2003.10769*, 2020.
 - [14] F. Nunnari, M. A. Kadir, and D. Sonntag, “On the overlap between grad-cam saliency maps and explainable visual features in skin cancer images,” in *International Cross-Domain Conference for Machine Learning and Knowledge Extraction*. Springer, 2021, pp. 241–253.
 - [15] T.-C. Hsieh, A. Bar-Haim, S. Moosa, N. Ehmke, K. W. Gripp, J. T. Pantel, M. Danyel, M. A. Mensah, D. Horn, S. Rosnev *et al.*, “Gestaltmatcher facilitates rare disease matching using facial phenotype descriptors,” Nature Publishing Group, Tech. Rep., 2022.
 - [16] “Home - Face2Gene,” Mar. 2022, [Online; accessed 5. May 2022]. [Online]. Available: <https://www.face2gene.com>
 - [17] “GestaltMatcher Database,” May 2022, [Online; accessed 5. May 2022]. [Online]. Available: <https://db.gestaltmatcher.org/publications>
 - [18] “Human Phenotype Ontology,” Apr. 2022, [Online; accessed 6. May 2022]. [Online]. Available: <https://hpo.jax.org/app>
 - [19] J. Deng, W. Dong, R. Socher, L.-J. Li, K. Li, and L. Fei-Fei, “Imagenet: A large-scale hierarchical image database,” in *2009 IEEE conference on computer vision and pattern recognition*. Ieee, 2009, pp. 248–255.
 - [20] D. Bau, B. Zhou, A. Khosla, A. Oliva, and A. Torralba, “Network dissection: Quantifying interpretability of deep visual representations,” in *Proceedings of the IEEE conference on computer vision and pattern recognition*, 2017, pp. 6541–6549.
 - [21] B. Kim, M. Wattenberg, J. Gilmer, C. Cai, J. Wexler, F. Viegas *et al.*, “Interpretability beyond feature attribution: Quantitative testing with concept activation vectors (tcav),” in *International conference on machine learning*. PMLR, 2018, pp. 2668–2677.
 - [22] N. Kokhlikyan, V. Miglani, M. Martin, E. Wang, B. Alsallakh, J. Reynolds, A. Melnikov, N. Kliushkina, C. Araya, S. Yan *et al.*, “Captum: A unified and generic model interpretability library for pytorch,” *arXiv preprint arXiv:2009.07896*, 2020.
 - [23] D. Matthew Zeiler and F. Rob, “Visualizing and understanding convolutional neural networks.” ECCV, 2014.

References

- [24] M. D. Zeiler, G. W. Taylor, and R. Fergus, “Adaptive deconvolutional networks for mid and high level feature learning,” in *2011 international conference on computer vision*. IEEE, 2011, pp. 2018–2025.
- [25] J. T. Springenberg, A. Dosovitskiy, T. Brox, and M. Riedmiller, “Striving for simplicity: The all convolutional net,” *arXiv preprint arXiv:1412.6806*, 2014.
- [26] A. Krizhevsky, I. Sutskever, and G. E. Hinton, “Imagenet classification with deep convolutional neural networks,” *Advances in neural information processing systems*, vol. 25, 2012.
- [27] Li, Andreeto, Ranzato, and Perona, “Caltech 101,” Apr 2022.
- [28] Griffin, Holub, and Perona, “Caltech 256,” Apr 2022.
- [29] M. Everingham, L. Van Gool, C. K. I. Williams, J. Winn, and A. Zisserman, “The PASCAL Visual Object Classes Challenge 2012 (VOC2012) Results,” <http://www.pascal-network.org/challenges/VOC/voc2012/workshop/index.html>.
- [30] K. Simonyan, A. Vedaldi, and A. Zisserman, “Deep inside convolutional networks: Visualising image classification models and saliency maps,” *arXiv preprint arXiv:1312.6034*, 2013.
- [31] O. Russakovsky, J. Deng, H. Su, J. Krause, S. Satheesh, S. Ma, Z. Huang, A. Karpathy, A. Khosla, M. Bernstein, A. C. Berg, and L. Fei-Fei, “ImageNet Large Scale Visual Recognition Challenge,” *International Journal of Computer Vision (IJCV)*, vol. 115, no. 3, pp. 211–252, 2015.
- [32] Y. Boykov and G. Funka-Lea, “Graph cuts and efficient nd image segmentation,” *International journal of computer vision*, vol. 70, no. 2, pp. 109–131, 2006.
- [33] E. Štrumbelj and I. Kononenko, “Explaining prediction models and individual predictions with feature contributions,” *Knowledge and information systems*, vol. 41, no. 3, pp. 647–665, 2014.
- [34] Y. LeCun, L. Bottou, Y. Bengio, and P. Haffner, “Gradient-based learning applied to document recognition,” *Proceedings of the IEEE*, vol. 86, no. 11, pp. 2278–2324, 1998.
- [35] R. R. Selvaraju, M. Cogswell, A. Das, R. Vedantam, D. Parikh, and D. Batra, “Grad-cam: Visual explanations from deep networks via gradient-based localization,” in *Proceedings of the IEEE international conference on computer vision*, 2017, pp. 618–626.
- [36] J. Zhang, S. A. Bargal, Z. Lin, J. Brandt, X. Shen, and S. Sclaroff, “Top-down neural attention by excitation backprop,” *International Journal of Computer Vision*, vol. 126, no. 10, pp. 1084–1102, 2018.
- [37] B. Zhou, A. Khosla, A. Lapedriza, A. Oliva, and A. Torralba, “Object detectors emerge in deep scene cnns,” *arXiv preprint arXiv:1412.6856*, 2014.
- [38] M. T. Ribeiro, S. Singh, and C. Guestrin, “" why should i trust you?" explaining the predictions of any classifier,” in *Proceedings of the 22nd ACM SIGKDD international conference on knowledge discovery and data mining*, 2016, pp. 1135–1144.

-
- [39] S. M. Lundberg and S.-I. Lee, “A unified approach to interpreting model predictions,” *Advances in neural information processing systems*, vol. 30, 2017.
 - [40] R. L. Draelos and L. Carin, “Hirescam: Faithful location representation in visual attention for explainable 3d medical image classification,” *arXiv preprint arXiv:2011.08891*, 2020.
 - [41] S. Srinivas and F. Fleuret, “Full-gradient representation for neural network visualization,” *Advances in neural information processing systems*, vol. 32, 2019.
 - [42] S. Hooker, D. Erhan, P.-J. Kindermans, and B. Kim, “Evaluating feature importance estimates,” 2018.
 - [43] A. Shrikumar, P. Greenside, and A. Kundaje, “Learning important features through propagating activation differences,” in *International conference on machine learning*. PMLR, 2017, pp. 3145–3153.
 - [44] M. Sundararajan, A. Taly, and Q. Yan, “Axiomatic attribution for deep networks,” in *International conference on machine learning*. PMLR, 2017, pp. 3319–3328.
 - [45] D. Smilkov, N. Thorat, B. Kim, F. Viégas, and M. Wattenberg, “Smoothgrad: removing noise by adding noise,” *arXiv preprint arXiv:1706.03825*, 2017.
 - [46] S. Y. Zhang, Zhifei and H. Qi, “Age progression/regression by conditional adversarial autoencoder,” in *IEEE Conference on Computer Vision and Pattern Recognition (CVPR)*. IEEE, 2017.
 - [47] J. Adebayo, J. Gilmer, M. Muelly, I. Goodfellow, M. Hardt, and B. Kim, “Sanity checks for saliency maps,” *Advances in neural information processing systems*, vol. 31, 2018.
 - [48] D. Alvarez-Melis and T. S. Jaakkola, “On the robustness of interpretability methods,” *arXiv preprint arXiv:1806.08049*, 2018.
 - [49] Y.-h. Sheu, “Illuminating the black box: interpreting deep neural network models for psychiatric research,” *Frontiers in Psychiatry*, vol. 11, p. 551299, 2020.
 - [50] C.-K. Yeh, C.-Y. Hsieh, A. Suggala, D. I. Inouye, and P. K. Ravikumar, “On the (in) fidelity and sensitivity of explanations,” *Advances in Neural Information Processing Systems*, vol. 32, 2019.
 - [51] S. Mohseni, N. Zarei, and E. D. Ragan, “A multidisciplinary survey and framework for design and evaluation of explainable ai systems,” *ACM Transactions on Interactive Intelligent Systems (TiiS)*, vol. 11, no. 3-4, pp. 1–45, 2021.
 - [52] Wikipedia contributors, “Likert scale — Wikipedia, the free encyclopedia,” 2022, [Online; accessed 6-November-2022]. [Online]. Available: https://en.wikipedia.org/w/index.php?title=Likert_scale&oldid=1109849563
 - [53] C. Molnar, *Interpretable Machine Learning*, 2019.

References

- [54] J. Deng, J. Guo, E. Ververas, I. Kotsia, and S. Zafeiriou, “Retinaface: Single-shot multi-level face localisation in the wild,” in *Proceedings of the IEEE/CVF conference on computer vision and pattern recognition*, 2020, pp. 5203–5212.
- [55] K. He, X. Zhang, S. Ren, and J. Sun, “Deep residual learning for image recognition,” in *Proceedings of the IEEE conference on computer vision and pattern recognition*, 2016, pp. 770–778.
- [56] D. Yi, Z. Lei, S. Liao, and S. Z. Li, “Learning face representation from scratch,” *arXiv preprint arXiv:1411.7923*, 2014.
- [57] M. B. Muhammad and M. Yeasin, “Eigen-cam: Class activation map using principal components,” in *2020 International Joint Conference on Neural Networks (IJCNN)*. IEEE, 2020, pp. 1–7.
- [58] A. C. Bovik, *The essential guide to image processing*. Academic Press, 2009.
- [59] K. Simonyan and A. Zisserman, “Very deep convolutional networks for large-scale image recognition,” *arXiv preprint arXiv:1409.1556*, 2014.
- [60] J. Gildenblat and contributors, “Pytorch library for cam methods,” <https://github.com/jacobgil/pytorchGradCam>, 2021.
- [61] A. Paszke, S. Gross, F. Massa, A. Lerer, J. Bradbury, G. Chanan, T. Killeen, Z. Lin, N. Gimelshein, L. Antiga *et al.*, “Pytorch: An imperative style, high-performance deep learning library,” *Advances in neural information processing systems*, vol. 32, 2019.
- [62] R. Hartley and A. Zisserman, *Multiple view geometry in computer vision*. Cambridge university press, 2003.
- [63] “Triangle: Definitions.” [Online]. Available: <https://www.cs.cmu.edu/~quake/triangle.defs.html>
- [64] S. Bach, A. Binder, G. Montavon, F. Klauschen, K.-R. Müller, and W. Samek, “On pixel-wise explanations for non-linear classifier decisions by layer-wise relevance propagation,” *PLoS ONE*, vol. 10, no. 7, p. e0130140, Jul. 2015.
- [65] D. Castelvecchi, “Can we open the black box of ai?” *Nature News*, vol. 538, no. 7623, p. 20, 2016.
- [66] S. Jetley, N. A. Lord, N. Lee, and P. H. S. Torr, “Learn to pay attention,” in *International Conference on Learning Representations*, 2018.
- [67] P. Linardatos, V. Papastefanopoulos, and S. Kotsiantis, “Explainable ai: A review of machine learning interpretability methods,” *Entropy*, vol. 23, no. 1, p. 18, 2021.
- [68] A. Santoro, D. Raposo, D. G. T. Barrett, M. Malinowski, R. Pascanu, P. W. Battaglia, and T. P. Lillicrap, “A simple neural network module for relational reasoning,” in *Advances in Neural Information Processing Systems*, vol. 30, 2017, pp. 4967–4976.

-
- [69] S. Tonekaboni, S. Joshi, M. D. McCradden, and A. Goldenberg, “What clinicians want: contextualizing explainable machine learning for clinical end use,” in *Machine learning for healthcare conference*. PMLR, 2019, pp. 359–380.
 - [70] X. Wang, R. Girshick, A. Gupta, and K. He, “Non-local neural networks,” in *2018 IEEE/CVF Conference on Computer Vision and Pattern Recognition*, 2018, pp. 7794–7803.
 - [71] B. Ait Skourt, A. El Hassani, and A. Majda, “Lung ct image segmentation using deep neural networks,” *Procedia Computer Science*, vol. 127, pp. 109–113, 2018, pROCEEDINGS OF THE FIRST INTERNATIONAL CONFERENCE ON INTELLIGENT COMPUTING IN DATA SCIENCES, ICDS2017. [Online]. Available: <https://www.sciencedirect.com/science/article/pii/S1877050918301157>
 - [72] S. Pereira, A. Pinto, V. Alves, and C. A. Silva, “Brain tumor segmentation using convolutional neural networks in mri images,” *IEEE transactions on medical imaging*, vol. 35, no. 5, pp. 1240–1251, 2016.
 - [73] C. Olah, A. Mordvintsev, and L. Schubert, “Feature visualization,” *Distill*, 2017, <https://distill.pub/2017/feature-visualization>.
 - [74] B. Zhou, A. Khosla, A. Lapedriza, A. Oliva, and A. Torralba, “Learning deep features for discriminative localization,” in *Proceedings of the IEEE conference on computer vision and pattern recognition*, 2016, pp. 2921–2929.
 - [75] Q. Ferry, J. Steinberg, C. Webber, D. R. FitzPatrick, C. P. Ponting, A. Zisserman, and C. Nellåker, “Diagnostically relevant facial gestalt information from ordinary photos,” *elife*, vol. 3, p. e02020, 2014.
 - [76] I. E. Nielsen, D. Dera, G. Rasool, N. Bouaynaya, and R. P. Ramachandran, “Robust explainability: A tutorial on gradient-based attribution methods for deep neural networks,” *arXiv preprint arXiv:2107.11400*, 2021.
 - [77] G. Montavon, A. Binder, S. Lapuschkin, W. Samek, and K.-R. Müller, “Layer-wise relevance propagation: an overview,” *Explainable AI: interpreting, explaining and visualizing deep learning*, pp. 193–209, 2019.
 - [78] L. Chen, J. Chen, H. Hajimirsadeghi, and G. Mori, “Adapting grad-cam for embedding networks,” in *Proceedings of the IEEE/CVF Winter Conference on Applications of Computer Vision*, 2020, pp. 2794–2803.
 - [79] N. Kokhlikyan, V. Miglani, M. Martin, E. Wang, B. Alsallakh, J. Reynolds, A. Melnikov, N. Kliushkina, C. Araya, S. Yan *et al.*, “A unified and generic model interpretability library for pytorch, 2020,” 2009.
 - [80] Z. Zhang, Y. Song, and H. Qi, “Age progression/regression by conditional adversarial autoencoder,” in *Proceedings of the IEEE conference on computer vision and pattern recognition*, 2017, pp. 5810–5818.
 - [81] A. Ghorbani, A. Abid, and J. Zou, “Interpretation of neural networks is fragile,” in *Proceedings of the AAAI conference on artificial intelligence*, vol. 33, no. 01, 2019, pp. 3681–3688.

References

- [82] R. Guidotti, A. Monreale, S. Ruggieri, F. Turini, F. Giannotti, and D. Pedreschi, “A survey of methods for explaining black box models,” *ACM Comput. Surv.*, vol. 51, no. 5, aug 2018. [Online]. Available: <https://doi.org/10.1145/3236009>
- [83] E. Tjoa and C. Guan, “A survey on explainable artificial intelligence (xai): Toward medical xai,” *IEEE Transactions on Neural Networks and Learning Systems*, vol. 32, no. 11, pp. 4793–4813, 2021.
- [84] V. Miglani, N. Kokhlikyan, B. Alsallakh, M. Martin, and O. Reblitz-Richardson, “Investigating saturation effects in integrated gradients,” *arXiv preprint arXiv:2010.12697*, 2020.
- [85] B. Zhou, A. Khosla, A. Lapedriza, A. Oliva, and A. Torralba, “Learning deep features for discriminative localization,” in *Proceedings of the IEEE conference on computer vision and pattern recognition*, 2016, pp. 2921–2929.
- [86] R. R. Hoffman, S. T. Mueller, G. Klein, and J. Litman, “Metrics for explainable ai: Challenges and prospects,” *arXiv preprint arXiv:1812.04608*, 2018.
- [87] A. Rosenfeld, “Better metrics for evaluating explainable artificial intelligence,” in *Proceedings of the 20th international conference on autonomous agents and multiagent systems*, 2021, pp. 45–50.
- [88] Y.-S. Lin, W.-C. Lee, and Z. B. Celik, “What do you see? evaluation of explainable artificial intelligence (xai) interpretability through neural backdoors,” *arXiv preprint arXiv:2009.10639*, 2020.
- [89] B. Kim, M. Wattenberg, J. Gilmer, C. Cai, J. Wexler, F. Viegas *et al.*, “Interpretability beyond feature attribution: Quantitative testing with concept activation vectors (tcav),” in *International conference on machine learning*. PMLR, 2018, pp. 2668–2677.